Radiation damage free ghost diffraction with atomic resolution

OPEN ACCESS
IOP Publishing
Journal of Physics B: Atomic, Molecular and Optical Physics
J. Phys. B: At. Mol. Opt. Phys. **51** (2018) 025503 (18pp)
https://doi.org/10.1088/1361-6455/aa9737

Radiation damage free ghost diffraction with atomic resolution

Zheng Li[1,2,3], **Nikita Medvedev**[1,4], **Henry N Chapman**[1,5,6] and **Yanhua Shih**[7]

[1] Center for Free-Electron Laser Science, DESY, Notkestraße 85, D-22607 Hamburg, Germany
[2] SLAC National Accelerator Laboratory, Menlo Park, CA 94025, United States of America
[3] Max Planck Institute for the Structure and Dynamics of Matter, D-22761 Hamburg, Germany
[4] Institute of Physics and Institute of Plasma Physics, Academy of Science of Czech Republic, Na Slovance 1999/2, 18221 Prague 8, Czechia
[5] Hamburg Centre for Ultrafast Imaging, Luruper Chaussee 149, D-22761 Hamburg, Germany
[6] Department of Physics, University of Hamburg, Jungiusstraße 9, D-20355 Hamburg, Germany
[7] Department of Physics, University of Maryland, Baltimore County, Baltimore, MD 21250, United States of America

E-mail: zheng.li@desy.de and shih@umbc.edu

Received 26 June 2017, revised 16 October 2017
Accepted for publication 31 October 2017
Published 21 December 2017

Abstract

The x-ray free electron lasers can enable diffractive structural determination of protein nanocrystals and single molecules that are too small and radiation-sensitive for conventional x-ray diffraction. However the electronic form factor may be modified during the ultrashort x-ray pulse due to photoionization and electron cascade caused by the intense x-ray pulse. For general x-ray imaging techniques, the minimization of the effects of radiation damage is of major concern to ensure reliable reconstruction of molecular structure. Here we show that radiation damage free diffraction can be achieved with atomic spatial resolution by using x-ray parametric down-conversion and ghost diffraction with entangled photons of x-ray and optical frequencies. We show that the formation of the diffraction patterns satisfies a condition analogous to the Bragg equation, with a resolution that can be as fine as the crystal lattice length scale of several Ångstrom. Since the samples are illuminated by low energy optical photons, they can be free of radiation damage.

Keywords: x-ray quantum optics, diffraction imaging, atomic resolution

(Some figures may appear in colour only in the online journal)

1. Introduction

The advent of femtosecond x-ray free electron lasers (XFELs) has enabled diffractive structural determination of protein nanocrystals and single molecules that are too small and radiation-sensitive for conventional x-ray diffraction [1–3]. Using x-ray pulses of ~10 fs, sufficient diffraction signals could be collected before significant structural changes occur in the sample [1]. Nevertheless, the electronic form factor could be modified due to photoionization and electron cascades caused by the intense x-ray pulse [4, 5]. For general x-ray imaging techniques, minimizing the effects of radiation damage is of major concern to guarantee a reliable reconstruction of the structure. Here we show that the radiation damage free diffraction is achievable with an atomic spatial resolution by using x-ray parametric down-conversion (XPDC) [6–8] and ghost diffraction with entangled photons of x-ray and optical frequencies. An intense hard x-ray pulse generated by an XFEL is used to pump a nonlinear medium, and is down-converted to two-photon pairs that consist of an x-ray and an optical photon with wavelengths λ_X and λ_o, respectively. The optical photons are sent to illuminate the sample crystals or molecules, and the reflected photons are

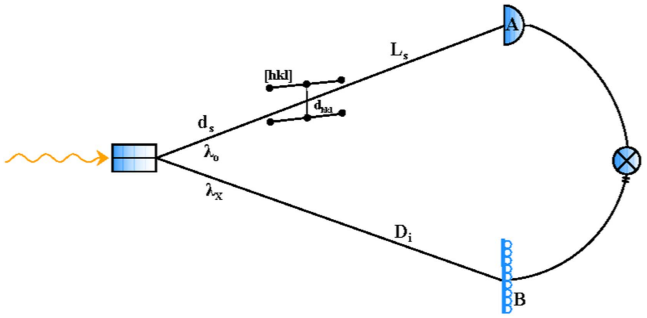

Figure 1. Proposed layout for two-color two-photon ghost diffraction using entangled x-ray and optical photon pairs from XPDC The optical photons with wavelength λ_o scatter off lattice planes with Miller index $[hkl]$ and inter-plane distance d_{hkl}, and are detected by the bucket detector D_A. The distances from the crystal plane to that XPDC output plane and the plane of bucket detector is d_s and L_s respectively. The entangled x-ray photons with wavelength λ_X travel a distance of D_i to the pixelated detector D_B. Correlation measurement is carried out for the detectors D_A and D_B.

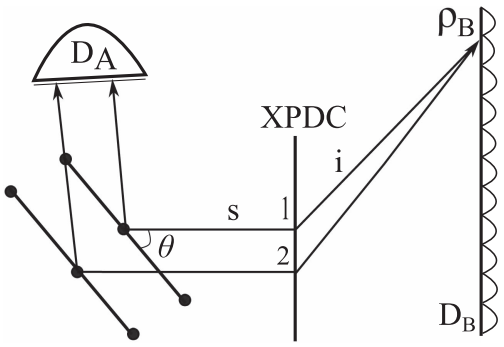

Figure 2. Unfolded two-photon diagram of the proposed experimental setup. The optical paths of the x-ray and optical photons are effectively concatenated at position 1 or 2 on the XPDC plane, because $\Delta(\vec{k}_s + \vec{k}_i) = 0$ and $\Delta(\vec{\rho}_s - \vec{\rho}_i) = 0$ are fulfilled at the same time for the two position-momentum entangled particles [16].

collected with a bucket detector D_A. The x-ray photons entangled with the optical photons travel a certain distance, and are captured by a pixel photon counting detector D_B. Based on the basic principle of ghost imaging [9–14], the output pulses of the bucket detector D_A and the pixel detector D_B are sent to a coincidence circuit with certain time gate for counting the joint detection of the two-photon pairs.

We show here that diffraction patterns can be formed by joint detection, and we illustrate that the formation of diffraction patterns satisfies a condition analogous to the Bragg equation with a resolution that could be as fine as the lattice length scale of several Ångstrom. Because the samples are illuminated by low energy optical photons, they can be free of radiation damage. The ultrabright intensity of XFELs could be crucial for realization of the proposed scheme to ensure sufficient two-photon flux and signal strength. Since the diffraction pattern formation is based on photon counting, the requirement for signal intensity is benign, we also show that the modified Bragg condition of the proposed ghost diffraction method can be satisfied with feasible experimental parameters.

2. Methods

In the proposed ghost diffraction scheme, optical photons and x-ray photons from XPDC are directed to illuminate a crystal in the optical arm and form diffraction patterns in the x-ray arm (figure 1). Without loss of generality, we assume that the signal photon has an optical wavelength of $\lambda_s = \lambda_o$, and the idler photon has an x-ray wavelength of $\lambda_i = \lambda_X$. The physical mechanism of the two-color entangled ghost diffraction can be understood from the particle nature of the optical and x-ray photons and their position-momentum entanglement. The optical photon of frequency ω scatters with the atoms in a nanocrystal or a molecule, and experiences momentum transfer $\vec{Q}$, with frequency independent Thomson scattering cross section $\frac{d\sigma(\vec{Q})}{d\Omega_{th}} = \frac{r_e^2}{2}(1 + \cos^2\theta)|f(\vec{Q})|^2$ provided that the optical photons are unpolarized, where r_e is the classical electron radius $r_e \simeq 2.82$ fm, and $f(\vec{Q})$ is the form factor. The elastic Rayleigh scattering of optical photon with the cross section $\frac{d\sigma(\vec{Q})}{d\Omega} \simeq r_e^2\,|f'(\omega) + if''(\omega)|^2 \propto \frac{\omega^4}{(\omega^2-\omega_0^2)^2}\frac{r_e^2}{2}(1 + \cos^2\theta)$ is equivalent to the dispersive corrections of form factor in the x-ray regime (see explanation in appendix A), which can be used for the phase retrieval in crystallography [15]. For photons as particles, the probability of reflection from an atom is in fact on the similar order of magnitude for the optical and x-ray photons. Without considering the molecular form factor of $f(\vec{Q})$, we could model the form factor of a crystal as periodic distributions of point scatterers as $f(\vec{Q}) = -r_e\delta(\vec{Q} - 2\pi\vec{G}_{hkl})$, where $\vec{G}_{hkl}$ is the reciprocal vector with $|\vec{G}_{hkl}| = \frac{1}{d_{hkl}}$. However, for the scattering of an optical photon on atoms, the momentum transfer $\vec{Q} = 2\frac{\omega}{c}\sin\theta(-\cos\phi\cos\theta, -\sin\phi\cos\theta, \sin\theta)$, which is proportional to the incident optical photon energy, is too small to form interference patterns at non-imaginary reflection angles because $\vec{Q} \ll \vec{G}_{hkl}$. Thus, Laue diffraction requires x-ray photons of wavelength $\lambda < 2d$.

In the entangled two-photon ghost diffraction, the momentum transfer can be effectively magnified from $\vec{Q}$ to $\tilde{m}\vec{Q}$ with a magnification factor of $\tilde{m} \sim 10^3$. The mechanism of momentum transfer magnification can be understood by a simple quantum model of the 'unfolded' two-photon ghost diffraction [17] (see figure 2). In this simplified model, we do not consider the transverse momenta of the down-converted photons. The photon fields on detectors D_A and D_B can be written in this case as

$$\hat{E}_A^{(+)} = \hat{a}_{1s}e^{ik_s r_{A1}} + \hat{a}_{2s}e^{ik_s r_{A2}}$$
$$\hat{E}_B^{(+)} = \hat{a}_{1i}e^{ik_i r_{B1}} + \hat{a}_{2i}e^{ik_i r_{B2}}, \quad (1)$$

where $\hat{a}_{lp}$, $l = 1, 2$, $p = s, i$ are the annihilation operators of signal and idler photons at position 1, 2 in figure 2. The

two-photon state $|\Psi\rangle$ can be expressed as

$$|\Psi\rangle = |0\rangle + \epsilon[\hat{a}_{1s}^{\dagger}\hat{a}_{1i}^{\dagger}e^{i\phi_1} + \hat{a}_{2s}^{\dagger}\hat{a}_{2i}^{\dagger}e^{i\phi_2}]|0\rangle, \quad (2)$$

where ϵ is the two-photon amplitude, and we can assume $\phi_1 = \phi_2$ since the pump beam from an XFEL or a synchrotron must be transversely coherent at position 1 and 2. The two-photon interference is formed due to the uncertainty in the birth place of the two-photon pair (either at position 1 or 2 in figure 2), and the property of the two-photon entangled state permits the uncertainty relation $\Delta(\vec{k}_s + \vec{k}_i) = 0$ and $\Delta(\vec{\rho}_s - \vec{\rho}_i) = 0$ to be satisfied at the same time [16], which guarantees the effective operation to concatenate the optical paths of the x-ray and optical photons exactly at the point of their birth positions. To keep the physical picture and expression simple for this illustrative discussion, we assume that the refractive index $n \sim 1$. It is straightforward to find the second-order coherence function $G_{AB} \propto \epsilon^2 \cos^2\left[\frac{\pi}{\lambda_s}(r_{A1} - r_{A2}) + \frac{\pi}{\lambda_i}(r_{B1} - r_{B2})\right]$, and Bragg peak is formed under condition

$$2d\sin\theta + \frac{\lambda_s}{\lambda_i}(r_{B1} - r_{B2}) = n\lambda_s. \quad (3)$$

In equation (3), the modified Bragg condition can be satisfied despite $d \ll \lambda_s$, because the optical path length difference can be compensated by that of the arm of idler photons magnified by a factor $\frac{\lambda_s}{\lambda_i}$ on the order of $\sim 10^3$. From the discussion above, we have an effective form factor $f_{\text{eff}}(\vec{Q}) = -r_e\delta(\tilde{m}\vec{Q} - 2\pi\vec{G}_{hkl})$, which is able to produce diffraction patterns for reciprocal vectors on the $1/\text{Å}$ scale.

3. Results

To establish the magnification effect on a solid basis, we carry out quantitative analysis of the resolving power of the proposed two-color ghost diffraction method. The refraction effect could be taken into account by employing the dynamical theory of diffraction, which treats the refraction explicitly and results in a shift of Laue point that depends on the refractive index of the crystal [18]. Denote the refractive index as $n(\omega) = 1 - n' - in''$, where $n' < 0$ for optical photons, the refractive index has a relation with the electric susceptibility $n(\omega) = \sqrt{1 + 4\pi\chi}$ [19], and χ can be determined by *ab initio* means for each atomic species at a given wavelength. From the detailed derivation presented in appendix B (equations (B.1)–(B.24)), as the optical photons scatter off lattice planes of inter-plane distance $d_{hkl} = d$, the condition for the x-ray photons to form peaks in the diffraction pattern is

$$\frac{2\tilde{m}d(\sin^2\theta - n')}{\sqrt{\sin^2\theta + 4\pi\chi}} = n\lambda_s, \quad (4)$$

for an integer n. θ is the reflection angle of the optical photon from the lattice planes of a Miller index $[hkl]$ (figure 3). The magnification factor $\tilde{m}$ is found to be (equation (B.23) in appendix)

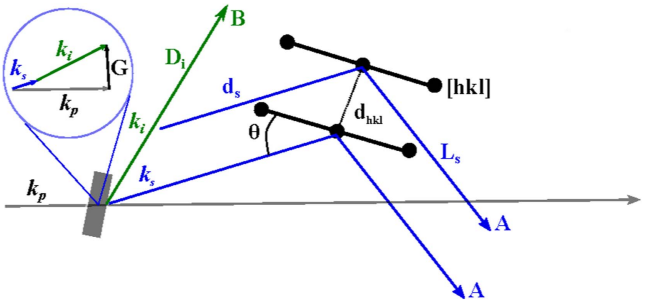

Figure 3. Sketch of the proposed experiment. The lattice plane of the sample forms an angle of θ with the incident optical photon in the arm A. The relative angle of the x-ray photon (arm B) with the pump photon is determined from the phase-matching diagram, $\vec{k}_s + \vec{k}_i = \vec{k}_p + \vec{G}$, where $\vec{G}$ is a reciprocal lattice vector orthogonal to certain atomic planes of a nonlinear crystal; $\vec{k}_s$, $\vec{k}_i$ and $\vec{k}_p$ are the wave vectors of the signal, idler and pump fields. And $z_s = d_s + L_s$, $z_i = D_i$ are the optical path lengths of the signal and idler photons.

$$\tilde{m} = 1 - \frac{|\vec{\rho}_B - \vec{d}|^2}{(\alpha + 1)\left(\frac{\lambda_i}{\lambda_s}\right)^2 D_i^2}, \quad (5)$$

where α is defined as $\frac{d_s}{D_i} = \alpha\frac{\lambda_i}{\lambda_s}$, and $\vec{\rho}_B$ is a position vector in the plane of the pixel detector. The magnification factor $\tilde{m}$ guarantees that the modified Bragg condition (equation (4)) can be satisfied in the case of $d \ll \lambda_s$. Note that the refraction effect could be neglected for the coherent diffractive imaging of single molecules, as shown in appendix C.

The two-photon coincidence counting rate of the bucket detector A and the pixel detector B can be written as [10, 12],

$$R_c(\vec{\rho}_B) = \frac{1}{T}\int dt_A dt_B S(t_B, t_A)\sigma_B \text{tr}_{\vec{\rho}_A}[\hat{E}_A^{(-)}\hat{E}_B^{(-)}\hat{E}_B^{(+)}\hat{E}_A^{(+)}\hat{\rho}], \quad (6)$$

where $S(t_B, t_A)$ is the coincidence gating function that vanishes unless $0 \leqslant t_B - t_A \leqslant T$, and describes the finite time gate of a joint detection of a two-photon pair [10]. $\vec{\rho}_A$ is a position vector on the plane of the bucket detector A, which has an area σ_A. And σ_B is the area of the pixel detector B. $\hat{\rho}$ is the density operator of the two-photon state on the output plane of the nonlinear crystal. $E_j^{(+)}$, $j = A, B$ is the positive frequency part of the photon field, and $E_j^{(-)} = (E_j^{(+)})^{\dagger}$. $\text{tr}_{\vec{\rho}_A}[\cdots]$ denotes the trace, i.e. coherent summation over $\vec{\rho}_A$. R_cT gives the pixelwise number of counted photons in one joint measurement. The photon fields at the plane of the bucket detector A and the pixel detector B, $\hat{E}_A^{(+)}$ and $\hat{E}_B^{(+)}$, can be expressed as

$$\hat{E}_A^{(+)} = \sum_{\vec{k}_s} g(\vec{\kappa}_s, \omega_s, \vec{\rho}_A, z_s)\hat{a}_s(\vec{k}_s)e^{-i\omega_s t_A}$$
$$\hat{E}_B^{(+)} = \sum_{\vec{k}_i} g(\vec{\kappa}_i, \omega_i, \vec{\rho}_B, z_i)\hat{a}_i(\vec{k}_i)e^{-i\omega_i t_B}, \quad (7)$$

where $z_s = d_s + L_s$ and $z_i = D_i$ are the full optical path lengths for the signal and the idler photon, $\vec{\kappa}$ is the transverse momentum of the photon field with $\vec{k} = \sqrt{k^2 - \kappa^2}\hat{e}_z + \vec{\kappa}$. $\hat{a}_p^{\dagger}(\vec{k})$ and $\hat{a}_p(\vec{k})$ are creation and annihilation operators of the

signal and the idler photon field in a specific mode at the output plane of the nonlinear crystal, with the commutator relation, $[\hat{a}_p(\vec{k}), \hat{a}_q^{\dagger}(\vec{k}')] = \delta_{p,q}\delta_{\omega,\omega'}\delta_{\vec{\kappa},\vec{\kappa}'}$. $g(\vec{\kappa}, \omega, \vec{\rho}, z)$ is the Green's function for a specific mode of the photon field. Assume two atoms in two lattice planes of Miller index $[hkl]$ with distance $d = d_{hkl}$ are in a plane a, $\vec{\rho}_a$ is a vector in this plane, and the photon–atom scattering amplitude is $t(\vec{\rho}_a)$, the photon fields $\hat{E}_A^{(+)}$ and $\hat{E}_B^{(+)}$ at the planes of detectors can be expressed as,

$$\begin{aligned}\hat{E}_A^{(+)} &= \sum_{\vec{k}_s}\int \mathrm{d}^2\vec{\rho}_{s'}\int \mathrm{d}^2\vec{\rho}_a \frac{-\mathrm{i}k_s}{2\pi \mathrm{d}_s}\mathrm{e}^{\mathrm{i}k_s \mathrm{d}_s}\mathrm{e}^{\mathrm{i}\vec{\kappa}_s\cdot\vec{\rho}_{s'}}\mathrm{e}^{\mathrm{i}\frac{k_s}{2\mathrm{d}_s}|\vec{\rho}_a-\vec{\rho}_{s'}|^2}\\ &\quad\times t(\vec{\rho}_a)\frac{-\mathrm{i}k_s}{2\pi L_s}\mathrm{e}^{\mathrm{i}k_s L_s}\mathrm{e}^{\mathrm{i}\frac{k_s}{2L_s}|\vec{\rho}_A-\vec{\rho}_a|^2}\mathrm{e}^{-\mathrm{i}\omega_s t_A}\hat{a}_s(\vec{k}_s)\\ \hat{E}_B^{(+)} &= \sum_{\vec{k}_i}\int \mathrm{d}^2\vec{\rho}_s \frac{-\mathrm{i}k_i}{2\pi D_i}\mathrm{e}^{\mathrm{i}k_i D_i}\mathrm{e}^{\mathrm{i}\vec{\kappa}_i\cdot\vec{\rho}_s}\mathrm{e}^{\mathrm{i}\frac{k_i}{2D_i}|\vec{\rho}_s-\vec{\rho}_B|^2}\mathrm{e}^{-\mathrm{i}\omega_i t_B}\hat{a}_i(\vec{k}_i).\end{aligned} \tag{8}$$

Using first-order perturbation theory, the two-photon amplitude from an XPDC process is (equation (B.10))

$$\begin{aligned}\langle 0|\hat{a}_s(\vec{k}_s)\hat{a}_i(\vec{k}_i)|\Psi\rangle &= -\mathrm{i}(2\pi)^3\gamma\delta(\nu_s+\nu_i)\\ &\quad\times\delta(\vec{\kappa}_s+\vec{\kappa}_i)\mathrm{sinc}\left(\nu_s D_{si}\frac{L}{2}\right),\end{aligned} \tag{9}$$

where $|\Psi\rangle$ is the two-photon state vector, and $\gamma = \frac{\chi^{(2)}E_p L}{2U_s U_i}\sqrt{\frac{\Omega_s\Omega_i T_s T_i c^2}{n_s n_i}}$, in which $\chi^{(2)}$ is the second-order susceptibility of the nonlinear crystal. U_j are the group velocities of the signal and the idler photons inside the nonlinear crystal of length L, T_j are their transmission coefficients, and E_p is the electric field strength of the pump field. Ω_s and Ω_i are the frequencies of the signal and the idler photons that satisfy the phase-matching condition $\omega_p n_p(\omega_p) - \Omega_s n_s(\Omega_s) - \Omega_i n_i(\Omega_i) = 0$. Provided that the modified Bragg equation (equation (4)) and the phase-matching condition are satisfied, diffraction patterns can be formed from the coincidence photon count in a joint measurement of the bucket detector D_A and the pixel detector D_B such that the reflection angle θ is measured with the detector D_A, and the corresponding intensity is measured with the detector D_B from coincidence counts on pixels of a given radius $|\vec{\rho}_B|$. For the schematic configuration in figure 1, the Bragg peaks are manifested as modulation of the coincident counting rate at $\vec{\rho}_B$ in the plane of the pixel detector with a background (see equations (B.26), (B.27) in appendix)

$$\begin{aligned}R_c(\vec{\rho}_B) &= \frac{1}{T}\int \mathrm{d}t_A \mathrm{d}t_B S(t_B, t_A)\sigma_B\left(\frac{\gamma\psi_0}{\pi\lambda_s R_s}\right)^2\\ &\quad\times\left|\int \mathrm{d}\nu_S \mathrm{e}^{\mathrm{i}\nu_S\tau_{BA}}\mathrm{sinc}\left(\nu_s D_{si}\frac{L}{2}\right)\right|^2\\ &\quad\times\cos^2\left[\frac{2\pi}{\lambda_s R_s}\vec{d}\cdot\left(\vec{\rho}_B-\frac{\vec{d}}{2}\right)\right],\end{aligned} \tag{10}$$

where γ and D_{si} are parameters of the XPDC process (see appendix B), $D_{si} = \frac{1}{U_s} - \frac{1}{U_i}$, and $\tau_{BA} = \tau_B - \tau_A$ with $\tau_i = t_i - \frac{r_i}{c}$, $i = A, B$. ψ_0 is the Thomson scattering amplitude of an atom in the lattice with the optical photons. And

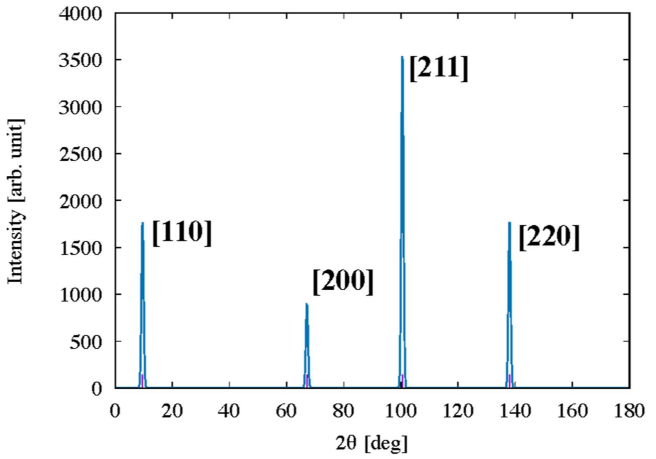

Figure 4. Simulated two-color two-photon ghost diffraction from a body centered cubic (bcc) crystal with lattice constant $a = b = c = 4$ Å. Optical photons of 3.1 eV are used to illuminate the sample crystal. Miller indices are labeled for the Bragg peaks. The broadening of Bragg peaks is determined by the Scherrer equation (equation (11)) for a nanocrystal of 100 nm size and refractive index $n = 1.2$.

$R_s = \frac{\lambda_i}{\lambda_s}D_i + d_s$ is the effective optical path length from the sample to the pixel detector B. We assume the phase-matching condition to be $\Omega_s n_s(\Omega_s) + \Omega_i n_i(\Omega_i) = ck_p$, and ignore $\vec{G}$ for simplicity, which can be restored for a given experimental configuration. The frequency of the signal field is $\omega_s = \Omega_s + \nu_s$, with ν_s characterizing the deviation from the central frequency Ω_s of the phase-matching condition, and $\nu_s = -\nu_i$.

For realistic experimental consideration, we assume that the entangled photon pair consists of an x-ray photon of energy 3.1 keV ($\lambda_i = 4$ Å) and an optical photon of energy of 3.1 eV ($\lambda_s = 4000$ Å). Nonlinear x-ray process with energy difference of two-photon pairs on such scale was experimentally demonstrated [6]. Assume the sample is placed at a distance of 1cm from the XPDC source, the reflection angle of optical photon is measured on detector D_A, and the x-ray photon in the two-photon pair is measured by the pixels with radius of 1 m on the pixel detector D_B placed at a distance of 10 m. In the XFEL nanocrystal diffraction experiment, virtual powder diffraction patterns are formed for various reflection angles. The single photons from the XPDC process have a certain angular spread [20]. It is practically advantageous to determine the actual reflection angle θ by a pixel detector D_A, although in an idealized setup the reflection angle can be uniquely determined by the geometrical configuration of the photon source and a single crystal, for which a bucket detector D_A is sufficient. The modified Bragg equation gives the ghost diffraction pattern in figure 4. The resolution requirement can be satisfied with the state-of-the-art pixel pnCCD detector that can achieve 75 μm pixel pitch [1]. The requirement for the spectral and angular resolution of the diffractometer is determined by $\frac{\Delta d}{d} + \cot\theta\Delta\theta = \frac{\Delta\lambda_s}{\lambda_s}$, which is on the same scale as the conventional Laue diffraction. For nanocrystals with the size L_c, the analogous Scherrer equation

is found to be (see appendix D, equations (D.1)–(D.4))

$$B = \frac{2\lambda_s(\sin^2\theta + 4\pi\chi)^{\frac{3}{2}}}{L_c\tilde{m}\sin\theta\cos\theta(\sin^2\theta + 4\pi\chi + \frac{n'}{2})}, \qquad (11)$$

which determines the width B of Bragg peaks. As shown figure 4, the width of Bragg peaks is on the same scale as Laue diffraction and is resolvable by the state-of-the-art diffractometer. The optical photon energy of 3.1 eV may fall below band gap of the crystal, thus significant absorption can be avoided. The proposed two-color entangled ghost diffraction approach could eventually achieve atomic resolution without radiation damage.

4. Discussion

It is important to notice, as the photon behaves as a point particle in the elastic scattering, its wavelength is irrelevant to the effective size of the photon, thus the optical photon does not smear out the crystal structure with a period that is much shorter than the photon wavelength. In fact the wavelength and the size of a quantum object reflect its wave-like and particle-like natures respectively, and should be distinguished one from another. It is known that the intensity of Bragg peaks should be reduced due to the dynamic structural factor $S(\vec{Q}, \omega_s)$ by a factor of $\exp\left\{-\frac{1}{2}\langle[\vec{Q}\cdot(\vec{u}_{\vec{R}}(t) - \vec{u}_{\vec{0}}(0))]^2\rangle_T\right\}$ [21], where $\vec{u}_{\vec{R}}(t)$ and $\vec{u}_{\vec{0}}(0)$ are the displacement vectors around $\vec{0}$ and $\vec{R}$, and $\vec{R}$ is the lattice vector, $\langle\cdots\rangle_T$ denotes the thermal expectation value. Due to the small momentum transfer $\vec{Q}$, the reduction of Bragg peak intensity in the entangled ghost diffraction is substantially weaker than that of the x-ray Laue diffraction.

Because the frequency of the optical photon is much lower than the x-ray photon, $\omega_o \ll \omega_X$, the experiment would suffer from strong absorption due to scattering of photon with bound electrons. Thus the optical photons in the vacuum ultraviolet regime is not favorable for the proposed ghost diffraction method. The entangled ghost diffraction scheme using optical photons to interact with the crystal could also potentially suffer from the skin effect when the samples are good conductors like copper, which has ~3 nm skin depth for optical photons in the visible and ultraviolet regime, and optical photons can only penetrate several uppermost lattice planes. In this sense, the proposed ghost diffraction scheme is suitable for diffractive structural determination of insulators, some semiconductors and proteins, which should have poor conductivity. For good conductors, our method is limited to the cases of thin and homogeneous samples, and the study of surfaces.

In order to achieve sufficient photon counting rate, it is crucially important to have an entangled two-photon source with high flux using x-ray quantum optical techniques [22]. Because the XPDC and the sum-frequency generation processes [6] are subject to the same nonlinear susceptibility, we can expect the feasibility of two-photon pair production with a similar $\frac{\lambda_s}{\lambda_i}$ ratio.

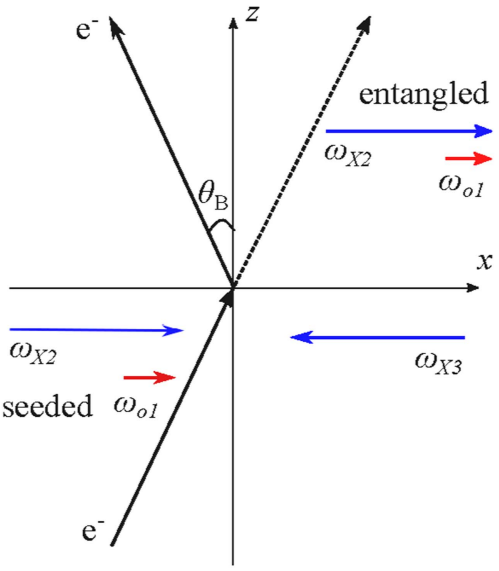

Figure 5. Sketch of the seeded Kapitza–Dirac-like XPDC process using single electron as the nonlinear medium. An x-ray photon of ω_{X3} is down-converted to two photons of frequencies ω_{o1} and ω_{X2}, as the electron is deflected with Bragg angle θ_B in coincidence. For the use of ghost diffraction, the down-converted photon pair can be then spatially separated by a metal foil that reflects the optical photon. The collinear geometry of k_{X3} and (k_{o1}, k_{X2}) can be loosened for more convenient experimental setup, provided the phase-matching condition is satisfied.

Consider the XPDC process $\omega_{X3} \rightarrow \omega_{X2} + \omega_{o1}$, which is physically equivalent to the Thomson scattering of x-rays by an atom illuminated with an optical field, Doppler-shifted sideband is induced by this process [23]. As elaborated in appendix E.1, the XPDC cross section from nonlinear crystal scales as $\frac{d\sigma^{(2)}}{d\Omega} \propto \omega_{o1}^{-1}$, and especially favors down-conversion to low energy optical photons. Using a semiclassical treatment [23, 24], we estimated the cross section of the instance in this work to be $\sim 1.9 \times 10^3$ fm^2 (see appendix E.1), which can be comparable to that of the Thomson scattering. We also show in appendix E.1 that the quasi-degenerate XPDC to pairs of two x-ray photons has a cross section that is four orders of magnitude lower than the XPDC to pairs of x-ray and optical photons. Moreover, the strong absorption of x-ray photons by the diamond crystal [8] and the radiation damage caused deterioration of phase-matching condition can significantly suppress the XPDC efficiency.

To overcome this problem, we could use radiation-hard multilayer metamaterials to enhance quantum efficiency of XPDC, or use compressed free electrons pulses directly as nonlinear medium for XPDC by the three-color Kapitza–Dirac-like mechanism (figure 5) [25]. Unlike SPDC of optical photons, which stems from the oscillation of bound electrons in the anharmonic potential around the atomic nuclei, the electron motion that dominantly contributes to XPDC is the figure-eight motion driven by the Lorentz force of electromagnetic field of intense x-rays, because the x-ray light has much smaller ponderomotive potential than the optical light. Since the figure-eight motion is in fact the same for free

electrons and electrons in nonlinear crystal, we can use single electrons directly as the nonlinear medium for XPDC. In appendix E.2, we used perturbation theory [25–27] to find the probability of the desired XPDC process under the phase-matching condition $\vec{k}_{X3} = \vec{k}_{o1} + \vec{k}_{X2}$ as

$$P(\omega_{o1}, \omega_{X2}, \omega_{X3}) = \left| \frac{v_z E_{o1} E_{X2} E_{X3}}{2c^2 \omega_{o1} \omega_{X2} \omega_{X3}} \right|^2 \delta(E_{fi}). \qquad (12)$$

In the three-color Kapitza–Dirac-like process, the electrons are scattered as $|\vec{p}_i\rangle \rightarrow |\vec{p}_f\rangle = |\vec{p}_i \pm (\vec{k}_{o1} + \vec{k}_{X2} + \vec{k}_{X3})\rangle$, $\delta(E_{fi}) = \delta(p_f^2/2 - p_i^2/2)$ ensures the energy conservation of the electrons, and v_z is the initial velocity of the electrons along the z axis. With electric field intensity $I \sim 10^{18}$ W cm^{-2} which is well below the QED critical intensity, and moderate electron velocity in non-relativistic regime, the XPDC probability could reach 10^{-5}.

5. Conclusions

In conclusion, we have theoretically described a mechanism to realize diffraction with atomic resolution by two-color entangled ghost diffraction. Because the sample is irradiated by photons of optical wavelength, the proposed scheme can be free of radiation damage by x-ray photons. In principle the proposed scheme could be applied for single molecules to determine the molecular structure using phase retrieval techniques of coherent diffractive imaging. Moreover, achieving resolution on a much smaller length scale than the wavelength of the illuminating photons using entangled state of particles opens up the possibility for future development of quantum optics based imaging techniques using various types of entangled particles, such as entangled photon-electron, electron-electron pair or electron-anti-neutrino pair from β-decay.

Acknowledgments

We thank the Hamburg Centre for Ultrafast Imaging for financial support. We thank Anton Classen, Todd Martínez, Jochen Schneider, Nina Rohringer, Ivan Vartanyants, Ralf Röhlsberger, Robin Santra, Oriol Vendrell, Jerome Hastings, David Reis, Shaul Mukamel, Lida Zhang, Xiaolei Zhu, Tao Peng, Liangliang Shi, Kareem Hegazy, Matthew Ware, Anton Classen, James Cryan, Matthias Fuchs and Andreas Kaldun for commenting on various aspects of the study. We are grateful for Sharon Shwartz and Christina Bömer for private communication and data of the on-going experiment of XPDC to entangled x-ray and optical photon pairs. ZL is thankful to the Volkswagen Foundation for the Peter Paul Ewald-Fellowship. Partial financial support from the Czech Ministry of Education (Grants LB15013 and LM2015083) is acknowledged by NM.

Table 1. Symbol table.

Symbol	Explanation
R_c	Counting rate of joint photon detection
$\|\Psi\rangle$	Two-photon state
$\hat{\rho}$	Density operator of the two-photon state on the output plane of the nonlinear medium
$\hat{E}_A^{(+)}$	Positive frequency part of the quantized photon field on the plane of bucket detector A
$\hat{E}_B^{(+)}$	Positive frequency part of the quantized photon field on the plane of pixel detector B
$\hat{E}_A^{(-)}$	Negative frequency part of the quantized photon field on the plane of bucket detector A
$\hat{E}_B^{(-)}$	Negative frequency part of the quantized photon field on the plane of pixel detector B
$\hat{a}_p^\dagger(\vec{k})$	Photon creation operator for specific mode $\vec{k}$ and channel p, $p = s, i$
$\hat{a}_p(\vec{k})$	Photon annihilation operator for specific mode $\vec{k}$ and channel p, $p = s, i$
$\vec{k}_s$	Wave vector of the signal photon of optical wavelength
$\vec{k}_i$	Wave vector of the idler photon of x-ray wavelength
k_s	$\|\vec{k}_s\|$
k_i	$\|\vec{k}_i\|$
$\vec{\kappa}_s$	Transverse momentum of the signal photon
$\vec{\kappa}_i$	Transverse momentum of the idler photon
$\vec{Q}$	Momentum transfer of the photon–atom scattering
λ_s	Wavelength of the signal photon
λ_i	Wavelength of the idler photon
$\vec{\rho}_A$	Position vector on the plane of bucket detector A
$\vec{\rho}_B$	Position vector on the plane of pixel detector B
$\vec{\rho}_a$	Position vector on the crystal plane of specific Miller index
$\vec{\rho}_s$	Position vector for the signal photon on the output plane of the nonlinear medium
$\vec{\rho}_{s'}$	Position vector for the idler photon on the output plane of the nonlinear medium
$\vec{d}$	Distance vector between two atoms in the crystal plane of specific Miller index
d	$\|\vec{d}\|$
d_s	Distance from the output plane of the nonlinear medium to the lattice plane of the crystal
L_s	Distance from the lattice plane to the bucket detector A
D_i	Distance from the output plane of the nonlinear medium to the pixel detector B
R_s	$d_s + \frac{\lambda_i}{\lambda_s} D_i$
z_s	$d_s + L_s$
z_i	D_i
ω_s	Frequency of the signal photon
ω_i	Frequency of the idler photon
Ω_s	Central frequency of the signal photon subject to phase-matching condition
Ω_i	Central frequency of the idler photon subject to phase-matching condition
U_{AB}	Joint photon detection amplitude
$V(\vec{\rho}_A, \vec{\rho}_B)$	Interference kernel in the joint photon detection amplitude
$G(\|\vec{\alpha}\|, \beta)$	$e^{i\frac{\beta}{2}\|\vec{\alpha}\|^2}$
δ	Difference of optical path lengths
θ	Reflection angle of the optical photon from the crystal
ψ_0	Photon–atom scattering amplitude
$\tilde{m}$	Magnification factor
$\mathcal{L}(\theta)$	Line shape of Bragg peak with reflection angle θ
L_c	Length of a nanocrystal

Appendix

The appendix is divided into the following sections. Appendix A explains the correspondence of the Thomson and the Rayleigh scattering in the x-ray and optical regime. Appendix B describes the derivation of the modified Bragg equation (equations (4) and (5) of the main text). Appendix C illustrates a simple kinematic description of Laue diffraction for the completeness of the theory presented in appendix B. In this section, we also present a Gedanken experiment of coherent diffraction imaging from a two-electron hydrogen-like molecule. Appendix D treats the broadening effect of Bragg peaks and derives the modified Scherrer equation. Appendix E elaborates the estimation of XPDC efficiency for the two proposed schemes, the one using diamond crystal and the another using single electron as the nonlinear medium. The symbols used in the appendix are listed in table 1.

Appendix A. Thomson and Rayleigh scattering in the optical and x-ray regime

In this section we elaborate the correspondence of Thomson and Rayleigh scattering in the x-ray and optical regimes. We show that the frequency independent Thomson scattering stays intact for both regimes, and the frequency dependent Rayleigh scattering in the optical regime is equivalent to the dispersive corrections of form factor in the x-ray regime.

We apply the Hamiltonian for photon-electron interaction under velocity gauge [19]

$$\begin{aligned}\hat{H}_{I1} &= -\frac{e}{m}\sum_{\vec{k},\vec{\epsilon}}\sqrt{\frac{2\pi\hbar}{\omega V}}\int \mathrm{d}^3r\ \hat{\Psi}^\dagger(\vec{r})[\vec{p}\cdot(\vec{\epsilon}\hat{a}_{\vec{k}\vec{\epsilon}}\mathrm{e}^{\mathrm{i}\vec{k}\cdot\vec{r}} \\ &\quad + \vec{\epsilon}^{\,*}\hat{a}^\dagger_{\vec{k}\vec{\epsilon}}\mathrm{e}^{-\mathrm{i}\vec{k}\cdot\vec{r}})\hat{\Psi}(\vec{r})]\hat{\Psi}(\vec{r}) \\ \hat{H}_{I2} &= \frac{\hbar\pi e^2}{mV}\sum_{\vec{k},\vec{\epsilon},\vec{k}',\vec{\epsilon}'}\frac{1}{\sqrt{\omega\omega'}}\int \mathrm{d}^3r\ \hat{\Psi}^\dagger(\vec{r}) \\ &\quad \times(\vec{\epsilon}^{\,*}\hat{a}^\dagger_{\vec{k}\vec{\epsilon}}\mathrm{e}^{-\mathrm{i}\vec{k}\cdot\vec{r}} + \vec{\epsilon}\hat{a}^\dagger_{\vec{k}\vec{\epsilon}}\mathrm{e}^{\mathrm{i}\vec{k}\cdot\vec{r}}) \\ &\quad \times(\vec{\epsilon}'\hat{a}_{\vec{k}'\vec{\epsilon}'}\mathrm{e}^{\mathrm{i}\vec{k}'\cdot\vec{r}} + \vec{\epsilon}'^{\,*}\hat{a}^\dagger_{\vec{k}'\vec{\epsilon}'}\mathrm{e}^{-\mathrm{i}\vec{k}'\cdot\vec{r}})\hat{\Psi}(\vec{r}),\end{aligned} \tag{A.1}$$

for the $\vec{p}\cdot\vec{A}$ and A^2 type interactions respectively. $\hat{\Psi}^{(\dagger)}$ and $\hat{a}^{(\dagger)}$ are the field operators for the electron and photon fields. $\vec{k}$, ω, $\vec{\epsilon}$ are the momentum, frequency and polarization vector of the photon. V is the quantization volume.

The A^2 type interaction from $\hat{H}_{I2}$ describes the Thomson scattering [19]. Assume the initial and final states are

$$\begin{aligned}|I\rangle &= |\Psi_a\rangle|N\rangle \\ |F\rangle &= \frac{1}{\sqrt{N}}|\Psi_a\rangle\hat{a}^\dagger_{\vec{k}_f\vec{\epsilon}_f}|N-1\rangle,\end{aligned} \tag{A.2}$$

where $|N\rangle$ denotes the Fock state of the photon field and $|\Psi_a\rangle$ is the electronic eigenstate of the molecule. Note in the summation $\sum_{\vec{k},\vec{\epsilon},\vec{k}',\vec{\epsilon}'}(\vec{\epsilon}^{\,*}\hat{a}^\dagger_{\vec{k}\vec{\epsilon}}\mathrm{e}^{-\mathrm{i}\vec{k}\cdot\vec{r}} + \vec{\epsilon}\hat{a}^\dagger_{\vec{k}\vec{\epsilon}}\mathrm{e}^{\mathrm{i}\vec{k}\cdot\vec{r}})\ (\vec{\epsilon}'\hat{a}_{\vec{k}'\vec{\epsilon}'}\mathrm{e}^{\mathrm{i}\vec{k}'\cdot\vec{r}} + \vec{\epsilon}'^{\,*}\hat{a}^\dagger_{\vec{k}'\vec{\epsilon}'}\mathrm{e}^{-\mathrm{i}\vec{k}'\cdot\vec{r}})$ for $\vec{k}=\vec{k}_i,\vec{k}_f$, $\vec{k}'=\vec{k}_i',\vec{k}_f'$, the terms of nonzero contribution to the transition is $[\hat{a}_{\vec{k}_i\vec{\epsilon}_i}\hat{a}^\dagger_{\vec{k}_f\vec{\epsilon}_f} + \hat{a}^\dagger_{\vec{k}_f\vec{\epsilon}_f}\hat{a}_{\vec{k}_i\vec{\epsilon}_i}]\mathrm{e}^{\mathrm{i}(\vec{k}_i-\vec{k}_f)\cdot\vec{r}}$. The transition matrix element can be calculated as

$$\begin{aligned}M_{I2} &= \frac{\pi\hbar e^2}{mV}\frac{(\vec{\epsilon}_i\cdot\vec{\epsilon}_f^{\,*})}{\sqrt{\omega_i\omega_f}}\langle N-1|\hat{a}_{\vec{k}_f\vec{\epsilon}_f}[2\hat{a}^\dagger_{\vec{k}_f\vec{\epsilon}_f}\hat{a}_{\vec{k}_i\vec{\epsilon}_i} \\ &\quad + \delta_{\vec{k}_f\vec{k}_i}\delta_{\vec{\epsilon}_f\vec{\epsilon}_i}]|N\rangle\int \mathrm{d}^3r\ \langle\Psi_a|\hat{\Psi}^\dagger(\vec{r})\mathrm{e}^{\mathrm{i}(\vec{k}_i-\vec{k}_f)\cdot\vec{r}}\hat{\Psi}|\Psi_a\rangle \\ &= \frac{2\pi\hbar e^2}{mV}\frac{\vec{\epsilon}_i\cdot\vec{\epsilon}_f^{\,*}}{\sqrt{\omega_i\omega_f}}f^{(0)}(\vec{Q}),\end{aligned} \tag{A.3}$$

where the form factor is

$$\begin{aligned}f^{(0)}(\vec{Q}) &= \int \mathrm{d}^3r\ \langle\Psi_a|\hat{\Psi}^\dagger(\vec{r})\hat{\Psi}(\vec{r})|\Psi_a\rangle\,\mathrm{e}^{\mathrm{i}\vec{Q}\cdot\vec{r}} \\ &= \int \mathrm{d}^3r\ \rho(\vec{r})\mathrm{e}^{\mathrm{i}\vec{Q}\cdot\vec{r}}\end{aligned} \tag{A.4}$$

for $\vec{Q}=\vec{k}_i-\vec{k}_f$. Fermi's golden rule gives the elastic Thomson cross section for $\omega=\omega_i=\omega_f$

$$\begin{aligned}J\mathrm{d}\sigma &= \frac{2\pi}{\hbar}\sum_{\vec{k}_f}|M_{I2}|^2\delta(\hbar(\omega_f-\omega_i)) \\ &= \frac{2\pi}{\hbar}\frac{V}{(2\pi)^3}\mathrm{d}\Omega\int \mathrm{d}k_f\ k_f^2|M_{I2}^2|\frac{1}{\hbar}\delta(\omega_f-\omega_i) \\ &= \frac{2\pi}{\hbar}\frac{V}{(2\pi)^3}\frac{1}{c^3}\frac{1}{\hbar}\mathrm{d}\Omega\int \mathrm{d}\omega_f\omega_f^2|M_{I2}|^2\delta(\omega_f-\omega_i) \\ &= \frac{2\pi}{\hbar}\frac{V}{(2\pi)^3}\frac{1}{c^3}\frac{\omega^2}{\hbar}\mathrm{d}\Omega|M_{I2}|^2 \\ \Rightarrow\frac{\mathrm{d}\sigma}{\mathrm{d}\Omega} &= \frac{V^2\omega^2}{4\pi^2c^4\hbar^2}|M_{I2}|^2 \\ &= \frac{e^4}{m^2c^4}|f^{(0)}(\vec{Q})|^2\sum_{\vec{\epsilon}_f}|\vec{\epsilon}_i\cdot\vec{\epsilon}_f^{\,*}|^2 \\ &= r_e^2|f^{(0)}(\vec{Q})|^2\frac{1}{2}(1+\cos^2\theta),\end{aligned} \tag{A.5}$$

where $J=c/V$ is the normalized photon flux per unit area and unit time. Thus the Thomson scattering remains the same for optical and x-ray photons because it is independent of the photon frequency.

Next we show the equivalence of Rayleigh scattering in optical regime to the dispersive correction of form factor $f'(\omega)+\mathrm{i}f''(\omega)$ in x-ray regime, such that the complete form factor is $f(\vec{Q},\omega)=f^{(0)}(\vec{Q})+f'(\omega)+\mathrm{i}f''(\omega)$. In the x-ray regime, the dispersive effects are used as a solution to the phase problem in crystallography [15, 28].

The Rayleigh scattering is described by the second-order interaction of $\vec{p}\cdot\vec{A}$ type. The corresponding transition matrix element is

$$
\begin{aligned}
M_{I1} = \frac{2\pi\hbar e^2}{mV}\frac{1}{\sqrt{\omega_i\omega_f}}\sum_r\Bigg\{&\langle\Psi_a|\int \mathrm{d}^3r\hat{\Psi}(\vec{r})\mathrm{e}^{-\mathrm{i}\vec{k}_f\cdot\vec{r}}\vec{p}\cdot\vec{\epsilon}_f^{\,*}\hat{\Psi}(\vec{r})|\Psi_r\rangle\frac{1}{E_a-E_r+\hbar\omega_i+\mathrm{i}\epsilon}\\
&\times\langle\Psi_r|\int \mathrm{d}^3r\hat{\Psi}(\vec{r})\mathrm{e}^{\mathrm{i}\vec{k}_i\cdot\vec{r}}\vec{p}\cdot\vec{\epsilon}_i\hat{\Psi}(\vec{r})|\Psi_a\rangle\\
&+\langle\Psi_a|\int \mathrm{d}^3r\hat{\Psi}(\vec{r})\mathrm{e}^{\mathrm{i}\vec{k}_i\cdot\vec{r}}\vec{p}\cdot\vec{\epsilon}_i\hat{\Psi}(\vec{r})|\Psi_r\rangle\\
&\times\frac{1}{E_a-E_r-\hbar\omega_i-\mathrm{i}\epsilon}\\
&\times\langle\Psi_r|\int \mathrm{d}^3r\hat{\Psi}(\vec{r})\mathrm{e}^{\mathrm{i}\vec{k}_i\cdot\vec{r}}\vec{p}\cdot\vec{\epsilon}_i\hat{\Psi}(\vec{r})|\Psi_a\rangle\Bigg\}\\
=\frac{2\pi\hbar e^2}{m\omega V}&[f'(\omega)+\mathrm{i}f''(\omega)],
\end{aligned}
\tag{A.6}
$$

where $|\Psi_r\rangle$ are the virtual states for the second-order transition. The dispersive corrections follow the standard definition in x-ray physics by decomposing the terms in the bracket of equation (A.6) using the identity $\frac{1}{x+\mathrm{i}\epsilon}=\mathrm{Pr}\frac{1}{x}-\mathrm{i}\pi\delta(x)$ [15, 19].

It can be shown that the matrix element of $\vec{p}\cdot\vec{A}$ interaction (equation (A.6)) relates to the classical Rayleigh scattering cross section in the optical regime, which has the $(\omega/\omega_0)^4$ dependence on the photon frequency. For this purpose, we reduce the model to a two-level system such that the classical *natural frequency* ω_0 can be defined through $\hbar\omega_0=E_r-E_a$, and assume dipole approximation $\mathrm{e}^{\mathrm{i}\vec{k}\cdot\vec{r}}\simeq 1$. Since $\omega\ll\omega_0$, we make expansion $\frac{1}{\omega_0+\omega}+\frac{1}{\omega_0-\omega}=\frac{1}{\omega_0}+\frac{\omega^2}{\omega_0^3}+\cdots$, and insert the expansion into equation (A.6), the matrix element reduces to

$$
\begin{aligned}
M_{I1} = -\frac{2\pi e^2}{mV}\frac{1}{\omega}\Bigg\{&\langle\Psi_a|\int \mathrm{d}^3r\hat{\Psi}(\vec{r})\vec{p}\cdot\vec{\epsilon}_f^{\,*}\hat{\Psi}(\vec{r})|\Psi_r\rangle\\
&\times\frac{1}{\omega_0}\langle\Psi_r|\int \mathrm{d}^3r\hat{\Psi}(\vec{r})\vec{p}\cdot\vec{\epsilon}_i\hat{\Psi}(\vec{r})|\Psi_a\rangle\\
&+\langle\Psi_a|\int \mathrm{d}^3r\hat{\Psi}(\vec{r})\vec{p}\cdot\vec{\epsilon}_i\hat{\Psi}(\vec{r})|\Psi_r\rangle\\
&\times\frac{1}{\omega_0}\langle\Psi_r|\int \mathrm{d}^3r\hat{\Psi}(\vec{r})\vec{p}\cdot\vec{\epsilon}_i\hat{\Psi}(\vec{r})|\Psi_a\rangle\Bigg\}\\
-\frac{2\pi e^2}{mV}\frac{\omega}{\omega_0^2}\Bigg\{&\langle\Psi_a|\int \mathrm{d}^3r\hat{\Psi}(\vec{r})\vec{p}\cdot\vec{\epsilon}_f^{\,*}\hat{\Psi}(\vec{r})|\Psi_r\rangle\\
&\times\frac{1}{\omega_0}\langle\Psi_r|\int \mathrm{d}^3r\hat{\Psi}(\vec{r})\vec{p}\cdot\vec{\epsilon}_i\hat{\Psi}(\vec{r})|\Psi_a\rangle\\
&+\langle\Psi_a|\int \mathrm{d}^3r\hat{\Psi}(\vec{r})\vec{p}\cdot\vec{\epsilon}_i\hat{\Psi}(\vec{r})|\Psi_r\rangle\\
&\frac{1}{\omega_0}\langle\Psi_r|\int \mathrm{d}^3r\hat{\Psi}(\vec{r})\vec{p}\cdot\vec{\epsilon}_i\hat{\Psi}(\vec{r})|\Psi_a\rangle\Bigg\}+\cdots.
\end{aligned}
\tag{A.7}
$$

Define the polarizibility tensor [29]

$$
\overleftrightarrow{\alpha}\overset{\mathrm{def}}{=}\frac{2}{\hbar}\sum_r\frac{\langle\Psi_a|\vec{p}|\Psi_r\rangle\langle\Psi_r|\vec{p}|\Psi_a\rangle}{\omega_a-\omega_r},
\tag{A.8}
$$

we can write equation (A.7) in a simple form

$$
M_{I1}\simeq\frac{2\pi\hbar e^2}{mV\omega}\vec{\epsilon}_i\overleftrightarrow{\alpha}\vec{\epsilon}_f^{\,*}+\frac{2\pi\hbar e^2\omega}{mV\omega_0^2}\vec{\epsilon}_i\overleftrightarrow{\alpha}\vec{\epsilon}_f^{\,*}+\cdots.
\tag{A.9}
$$

We take constant polarization approximation that $\overleftrightarrow{\alpha}=\alpha_0\overleftrightarrow{\mathbb{I}}$, and equation (A.9) gives

$$
M_{I1}\simeq\frac{2\pi\hbar e^2\alpha_0}{mV\omega}(\vec{\epsilon}_i\cdot\vec{\epsilon}_f^{\,*})+\frac{2\pi\hbar e^2\alpha_0\omega}{mV\omega_0^2}(\vec{\epsilon}_i\cdot\vec{\epsilon}_f^{\,*})+\cdots.
\tag{A.10}
$$

Without considering interference between the two terms in equation (A.10), it gives the Rayleigh scattering cross section of second-order $\vec{p}\cdot\vec{A}$ interaction in the optical regime, and recall its form in the x-ray regime in equation (A.6),

$$
\begin{aligned}
\frac{\mathrm{d}\sigma}{\mathrm{d}\Omega}&=\frac{V^2\omega^2}{4\pi^2c^4\hbar^2}|M_{I1}|^2\\
&=r_e^2\left[\alpha_0^2\left(1+\frac{\omega_4}{\omega_0^4}\right)\right]\frac{1}{2}(1+\cos^2\theta)\\
&=r_e^2|f'(\omega)+\mathrm{i}f''(\omega)|^2.
\end{aligned}
\tag{A.11}
$$

From equation (A.11) we could conceive the usage of Rayleigh scattering in the entangled optical x-ray ghost diffraction, as it is applied to the phase problem of x-ray crystallography.

Appendix B. Modified Bragg equation for two-color two-photon diffraction

We assume paraxial approximation for the wave vectors of modes $|\vec{k}\rangle$ of the photon field, $\vec{k}=\sqrt{k^2-\kappa^2}\,\hat{e}_z+\vec{\kappa}$, with $k=\frac{\omega}{c}\gg\kappa$ and $\vec{\kappa}=(k_x, k_y, 0)$. The two-photon coincidence counting rate of the bucket detector A and the pixel detector can be written as [8, 10, 12],

$$
R_c(\vec{\rho}_B)=\frac{1}{T}\int \mathrm{d}t_A\mathrm{d}t_B S(t_B, t_A)\sigma_B\mathrm{tr}_{\vec{\rho}_A}[\hat{E}_A^{(-)}\hat{E}_B^{(-)}\hat{E}_B^{(+)}\hat{E}_A^{(+)}\hat{\rho}],
\tag{B.1}
$$

where $S(t_B, t_A)$ is the coincidence gating function that vanishes unless $0 \leqslant t_B - t_A \leqslant T$ and can be approximated as a rectangular function, $\vec{\rho}_A$ and $\vec{\rho}_B$ are vectors on the plane of the bucket detector A with an area σ_A, the plane of the pixel detector B with an area σ_B respectively. $\hat{\rho}$ is the density operator of the two-photon state on the output plane of the nonlinear crystal. $\hat{E}_j^{(+)}$, $j = A, B$ is the positive frequency part of the photon field, and $\hat{E}_j^{(-)} = (\hat{E}_j^{(+)})^\dagger$. And $\mathrm{tr}_{\vec{\rho}_A}[\cdots]$ denotes the trace and coherent summation over $\vec{\rho}_A$. We compute the photon fields at the plane of the bucket detector A and the pixel detector B, $\hat{E}_A^{(+)}$ and $\hat{E}_B^{(+)}$ as,

$$\begin{aligned}\hat{E}_A^{(+)}(\vec{\kappa}_s, \vec{k}_s, \vec{\rho}_A, z_s, \omega_s, t_A) &= \sum_{\vec{k}_s} g(\vec{\kappa}_s, \omega_s, \vec{\rho}_A, z_s)\hat{a}_s(\vec{k}_s)\mathrm{e}^{-\mathrm{i}\omega_s t_A}\\ \hat{E}_B^{(+)}(\vec{\kappa}_i, \vec{k}_i, \vec{\rho}_B, z_i, \omega_i, t_B) &= \sum_{\vec{k}_i} g(\vec{\kappa}_i, \omega_i, \vec{\rho}_B, z_i)\hat{a}_i(\vec{k}_i)\mathrm{e}^{-\mathrm{i}\omega_i t_B},\end{aligned} \tag{B.2}$$

where $z_s = d_s + L_s$ and $z_i = D_i$ are the full optical path lengths for the signal and the idler photons. $\hat{a}_p^\dagger(\vec{k})$ and $\hat{a}_p(\vec{k})$ are operators of signal and idler photon fields in a specific mode at the output plane of the nonlinear crystal, with the commutator relation,

$$[\hat{a}_p(\vec{k}), \hat{a}_q^\dagger(\vec{k}')] = \delta_{p,q}\delta_{\omega,\omega'}\delta_{\vec{\kappa},\vec{\kappa}'}. \tag{B.3}$$

$g(\vec{\kappa}, \omega, \vec{\rho}, z)$ is the Green's function for a specific mode of photon field.

Assume two atoms in two lattice planes of Miller index $[hkl]$ with the distance $d = d_{hkl}$ are in a plane a, $\vec{\rho}_a$ is a vector in this plane (figure B1), and the photon–atom scattering amplitude is $t(\vec{\rho}_a)$, $\hat{E}_A^{(+)}$ and $\hat{E}_B^{(+)}$ can be written as [12],

$$\begin{aligned}\hat{E}_A^{(+)} &\equiv \hat{E}_A^{(+)}(\vec{\kappa}_s, \vec{k}_s, \vec{\rho}_A, z_s, \omega_s, t_A)\\ &= \sum_{\vec{k}_s}\int \mathrm{d}^2\vec{\rho}_{s'}\int \mathrm{d}^2\vec{\rho}_a \frac{-\mathrm{i}k_s}{2\pi d_s}\mathrm{e}^{\mathrm{i}k_s d_s}\mathrm{e}^{\mathrm{i}\vec{\kappa}_{s'}\cdot\vec{\rho}_{s'}}\\ &\quad\times \mathrm{e}^{\mathrm{i}\frac{k_s}{2d_s}|\vec{\rho}_a-\vec{\rho}_{s'}|^2}t(\vec{\rho}_a)\frac{-\mathrm{i}k_s}{2\pi L_s}\mathrm{e}^{\mathrm{i}k_s L_s}\mathrm{e}^{\mathrm{i}\frac{k_s}{2L_s}|\vec{\rho}_A-\vec{\rho}_a|^2}\\ &\quad\times \mathrm{e}^{-\mathrm{i}\omega_s t_A}\hat{a}_s(\vec{k}_s)\\ \hat{E}_B^{(+)} &\equiv \hat{E}_B^{(+)}(\vec{\kappa}_i, \vec{k}_i, \vec{\rho}_B, z_i, \omega_i, t_B)\\ &= \sum_{\vec{k}_i}\int \mathrm{d}^2\vec{\rho}_s \frac{-\mathrm{i}k_i}{2\pi D_i}\mathrm{e}^{\mathrm{i}k_i D_i}\mathrm{e}^{\mathrm{i}\vec{\kappa}_i\cdot\vec{\rho}_s}\mathrm{e}^{i\frac{k_i}{2D_i}|\vec{\rho}_s-\vec{\rho}_B|^2}\\ &\quad\times \mathrm{e}^{-\mathrm{i}\omega_i t_B}\hat{a}_i(\vec{k}_i).\end{aligned} \tag{B.4}$$

Denote $G(|\vec{\alpha}|, \beta) = \mathrm{e}^{\mathrm{i}\frac{\beta}{2}|\vec{\alpha}|^2}$, its two-dimensional Fourier transformation is

$$\int \mathrm{d}^2\vec{\alpha}G(|\vec{\alpha}|, \beta)\mathrm{e}^{\mathrm{i}\vec{\gamma}\cdot\vec{\alpha}} = \mathrm{i}\frac{2\pi}{\beta}G\left(|\vec{\gamma}|, -\frac{1}{\beta}\right). \tag{B.5}$$

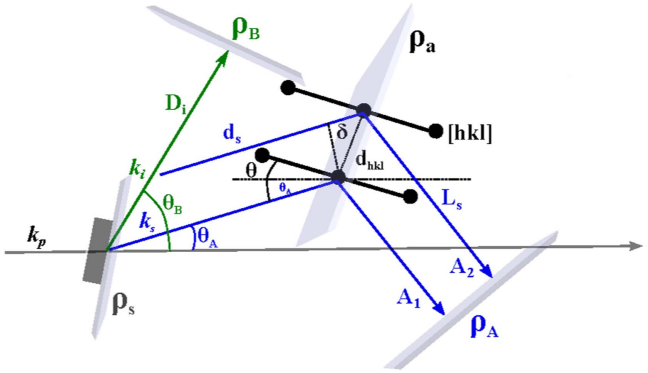

Figure B1. Proposed layout for two-color two-photon ghost diffraction using entangled x-ray and optical photon pair. $\vec{\rho}_A$, $\vec{\rho}_B$, $\vec{\rho}_s$, $\vec{\rho}_a$ are vectors on the planes of the bucket detector A, the pixel detector B, the x-ray PDC source and atoms in the sample. The path of the optical photon in the arm A is labeled by blue lines, with the distance d_s from the XPDC plane to the crystal plane and the distance from L_s to the bucket detector A. The path of the x-ray photon in the arm B is labeled by green line, with the distance D_i from the XPDC plane to the pixel detector B. k_p, k_s and k_i are the momentum vectors of the pump, the signal (optical) and the idler (x-ray) photons.

The photon fields $\hat{E}_A^{(+)}$ and $\hat{E}_B^{(+)}$ can be then written as

$$\begin{aligned}\hat{E}_A^{(+)} &= \sum_{\vec{k}_s}\int \mathrm{d}^2\vec{\rho}_a \frac{1}{\mathrm{i}\lambda_s L_s}t(\vec{\rho}_a)G\left(|\vec{\rho}_a - \vec{\rho}_A|, \frac{k_s}{L_s}\right)\\ &\quad\times \mathrm{e}^{\mathrm{i}\vec{\kappa}_s\cdot\vec{\rho}_a}G\left(|\vec{\kappa}_s|, -\frac{d_s}{k_s}\right)\mathrm{e}^{\mathrm{i}(k_s z_s - \omega_s t_A)}\hat{a}_s(\vec{k}_s)\\ \hat{E}_B^{(+)} &= \sum_{\vec{k}_i} G\left(|\vec{\kappa}_i|, -\frac{D_i}{k_i}\right)\mathrm{e}^{\mathrm{i}\vec{\kappa}_i\cdot\vec{\rho}_B}\mathrm{e}^{\mathrm{i}(k_i z_i - \omega_i t_B)}\hat{a}_i(\vec{k}_i).\end{aligned} \tag{B.6}$$

With equation (B.6), we can obtain explicitly the second-order coherence function in equation (B.1),

$$\begin{aligned}G_{AB} &= \mathrm{tr}_{\vec{\rho}_A}[\hat{E}_A^{(-)}\hat{E}_B^{(-)}\hat{E}_B^{(+)}\hat{E}_A^{(+)}\hat{\rho}]\\ &= \left|\int \mathrm{d}^2\vec{\rho}_A\langle 0|\hat{E}_B^{(+)}\hat{E}_A^{(+)}|\Psi\rangle\right|^2\\ &\equiv \left|\int \mathrm{d}^2\vec{\rho}_A U_{AB}\right|^2,\end{aligned} \tag{B.7}$$

where $|\Psi\rangle$ is the two-photon state vector, and U_{AB} is the joint photon detection amplitude. Without loss of generality, we ignore here the reciprocal lattice vector $\vec{G}$ of the nonlinear crystal, which can be added for a given experimental configuration. Suppose the phase-matching condition is satisfied for $\omega_p n_p(\omega_p) - \Omega_s n_s(\Omega_s) - \Omega_i n_i(\Omega_i) = 0$, with $K_j = \frac{\Omega_j}{c}$, and deviation from the central frequency $\omega_j = \Omega_j + \nu_j$, $j = s, i$. Frequency and spatial filtering guarantees $\nu_j \ll \Omega_j$ and $\kappa_j \ll K_j$, thus we have

$$\begin{aligned}\vec{k}_j &= \vec{\kappa}_j + \left(K_j + \frac{\nu_j}{c} + \frac{\nu_j^2}{2\Omega_j c} - \frac{\kappa_j^2}{2K_j}\right)\hat{e}_z\\ &\simeq \vec{\kappa}_j + \left(K_j + \frac{\nu_j}{c}\right)\hat{e}_z.\end{aligned} \tag{B.8}$$

Taken equations (B.6) and (B.7), we have

$$U_{AB} = \frac{1}{\mathrm{i}\lambda_s L_s} \mathrm{e}^{\mathrm{i}(K_s z_s + K_i z_i - \Omega_s t_A - \Omega_i t_B)} \times \left[\sum_{\vec{k}_s, \vec{k}_i} g'_A(\vec{\rho}_A, \nu_s, \vec{\kappa}_s) g'_B(\vec{\rho}_B, \nu_i, \vec{\kappa}_i) \langle 0 | \hat{a}_s(\vec{k}_s) \hat{a}_i(\vec{k}_i) | \Psi \rangle \right] \equiv \frac{1}{\mathrm{i}\lambda_s L_s} \mathrm{e}^{\mathrm{i}(K_i z_i - \Omega_s t_A - \Omega_i t_B)} U'. \tag{B.9}$$

Using a first-order perturbation theory, the two-photon amplitude from a PDC process is shown to be [12, 30],

$$\langle 0 | \hat{a}_s(\vec{k}_s) \hat{a}_i(\vec{k}_i) | \Psi \rangle = -\mathrm{i}(2\pi)^3 \gamma \delta(\nu_s + \nu_i) \times \delta(\vec{\kappa}_s + \vec{\kappa}_i) \mathrm{sinc}\left(\nu_s D_{si} \frac{L}{2} \right), \tag{B.10}$$

where $\gamma = \frac{\chi^{(2)} E_p L}{2 U_s U_i} \sqrt{\frac{\Omega_s \Omega_i T_s T_i c^2}{n_s n_i}}$, $D_{si} = \frac{1}{U_s} - \frac{1}{U_i}$, U_s and U_i are the group velocity of the signal and the idler photons inside the nonlinear crystal of length L $\chi^{(2)}$ is the second-order susceptibility of the nonlinear crystal, U_j is the group velocity of the signal and the idler photons inside the nonlinear crystal of length L, T_j are their transmission coefficients, and E_p is the strength of the pump field. Using the relation

$$\sum_{\vec{k}_s} \to \frac{V_Q}{(2\pi)^3} \int \mathrm{d}\vec{k}_s = \frac{V_Q}{(2\pi)^3} \int \mathrm{d}^2 \vec{\kappa}_s \times \int \mathrm{d}\omega_s \frac{\mathrm{d}k_{s,z}}{d\omega_s} = \frac{V_Q}{(2\pi)^3 c} \int \mathrm{d}^2 \vec{\kappa}_s \int \mathrm{d}\nu_s, \tag{B.11}$$

$$\hat{a}_s(\vec{k}_s) \to \frac{c}{V_Q} \hat{a}_s(\vec{\kappa}_s, \nu_s), \tag{B.12}$$

where V_Q is the quantization volume. We can write U' in equation (B.9) as

$$\begin{aligned} U' = {} & -\mathrm{i}(2\pi)^{-3} \gamma \int \mathrm{d}\nu_s \mathrm{e}^{\mathrm{i}\nu_s \tau_{BA}} \mathrm{sinc}\left(\nu_s D_{si} \frac{L}{2} \right) \int \mathrm{d}^2 \vec{\rho}_a \\ & \times \int \mathrm{d}^2 \vec{\kappa}_s G\left(|\vec{\kappa}_s|, -\frac{D_i}{k_i} \right) \mathrm{e}^{-\mathrm{i}\vec{\kappa}_s \cdot \vec{\rho}_B} \\ & \times G\left(|\vec{\kappa}_s|, -\frac{d_s}{k_s} \right) \mathrm{e}^{\mathrm{i}\vec{\kappa}_s \cdot \vec{\rho}_a} t(\vec{\rho}_a) G\left(|\vec{\rho}_a|, \frac{k_s}{L_s} \right) G\left(|\vec{\rho}_A|, \frac{k_s}{L_s} \right) \\ & \times \mathrm{e}^{-\mathrm{i}\frac{k_s}{L_s} \vec{\rho}_a \cdot \vec{\rho}_A} \mathrm{e}^{\mathrm{i}K_s z_s} \\ \equiv {} & -\mathrm{i}\gamma \int \mathrm{d}\nu_s \mathrm{e}^{\mathrm{i}\nu_s \tau_{BA}} \mathrm{sinc}\left(\nu_s D_{si} \frac{L}{2} \right) \int \mathrm{d}^2 \vec{\rho}_a I_{\vec{\kappa}_s} \\ & \times t(\vec{\rho}_a) G\left(|\vec{\rho}_a|, \frac{k_s}{L_s} \right) G\left(|\vec{\rho}_A|, \frac{k_s}{L_s} \right) \\ & \times \mathrm{e}^{-\mathrm{i}\frac{k_s}{L_s} \vec{\rho}_a \cdot \vec{\rho}_A} \mathrm{e}^{\mathrm{i}K_s z_s}, \end{aligned} \tag{B.13}$$

where $\tau_{BA} = \tau_B - \tau_A$, $\tau_i = t_i - \frac{r_i}{c}$, $i = A, B$, and r_i are the full lengths of the optical paths. Define the effective sample-to-pixel detector path length $R_s = d_s + \frac{\lambda_i}{\lambda_s} D_i$, the integral $I_{\vec{\kappa}_s}$ over transverse momentum $\vec{\kappa}_s$ in equation (B.13) can be rewritten as

$$\begin{aligned} I_{\vec{\kappa}_s} &= \frac{1}{(2\pi)^3} \int \mathrm{d}^2 \vec{\kappa}_s G\left(|\vec{\kappa}_s|, -\left(\frac{D_i}{k_i} + \frac{d_s}{k_s} \right) \right) \mathrm{e}^{\mathrm{i}\vec{\kappa}_s \cdot (\vec{\rho}_a - \vec{\rho}_B)} \\ &= \frac{1}{(2\pi)^3} (-\mathrm{i}) \frac{2\pi}{\frac{D_i}{k_i} + \frac{d_s}{k_s}} G\left(|\vec{\rho}_a - \vec{\rho}_B|, \frac{1}{\frac{D_i}{k_i} + \frac{d_s}{k_s}} \right) \\ &= \frac{1}{2\pi} \frac{1}{\mathrm{i}\lambda_s R_s} G\left(|\vec{\rho}_a - \vec{\rho}_B|, \frac{K_s}{R_s} \right), \end{aligned} \tag{B.14}$$

because $\frac{D_i}{k_i} + \frac{d_s}{k_s} = \frac{1}{2\pi}(D_i \lambda_i + d_s \lambda_s) = \frac{\lambda_s}{2\pi}(D_i \frac{\lambda_i}{\lambda_s} + d_s) = \frac{R_s}{K_s}$. The amplitude for joint photon detection at the bucket detector A and the pixel detector B is then

$$\begin{aligned} U_{AB} = \langle 0 | \hat{E}_B^{(+)} \hat{E}_A^{(+)} | \Psi \rangle = {} & -\frac{\gamma}{\lambda_s L_s} \mathrm{e}^{\mathrm{i}(K_i z_i - \Omega_s t_A - \Omega_i t_B)} \\ & \times \int \mathrm{d}\nu_s \mathrm{e}^{\mathrm{i}\nu_s \tau_{BA}} \mathrm{sinc}\left(\nu_s D_{si} \frac{L}{2} \right) \\ & \times \left\{ \frac{\mathrm{e}^{\mathrm{i}K_s z_s}}{2\pi \mathrm{i}\lambda_s R_s} G\left(|\vec{\rho}_A|, \frac{K_s}{L_s} \right) G\left(|\vec{\rho}_B|, \frac{K_s}{R_s} \right) \right. \\ & \times \int \mathrm{d}^2 \vec{\rho}_a t(\vec{\rho}_a) G\left(|\vec{\rho}_a|, K_s \left(\frac{1}{L_s} + \frac{1}{R_s} \right) \right) \\ & \left. \times \mathrm{e}^{-\mathrm{i}K_s \left(\frac{\vec{\rho}_B}{R_s} + \frac{\vec{\rho}_A}{L_s} \right) \cdot \vec{\rho}_a} \right\} \\ \equiv {} & -\frac{\gamma}{\lambda_s L_s} \mathrm{e}^{\mathrm{i}(K_i z_i - \Omega_s t_A - \Omega_i t_B)} \int \mathrm{d}\nu_s \mathrm{e}^{\mathrm{i}\nu_s \tau_{BA}} \\ & \times \mathrm{sinc}\left(\nu_s D_{si} \frac{L}{2} \right) V(\vec{\rho}_A, \vec{\rho}_B), \end{aligned} \tag{B.15}$$

where $V(\vec{\rho}_A, \vec{\rho}_B)$ is the interference kernel of the joint photon detection amplitude U_{AB} that characterizes the formation of the two-photon diffraction pattern. We now consider the scattering of the optical photon with the atoms in a lattice by integrating over $\vec{\rho}_a$, and the collection of optical photons at the bucket detector A by integrating over $\vec{\rho}_A$ in the detector plane, because the bucket detector collects photons without distinguishing their actual position. We expect that diffraction patterns can be formed on the image plane of the pixel detector B, with intensity $I(\vec{\rho}_B)$ and joint photon counting rate $R_c(\vec{\rho}_B)$ at $\vec{\rho}_B$

$$I(\vec{\rho}_B) = R_c(\vec{\rho}_B) T \sim \left| \int \mathrm{d}^2 \vec{\rho}_A V(\vec{\rho}_A, \vec{\rho}_B) \right|^2. \tag{B.16}$$

To obtain the analog of Bragg equation for the two-color two-photon ghost diffraction, we consider two optical paths A_1 and A_2 of the optical photons that scatter with two atoms in adjacent lattice planes with distance $d \equiv d_{hkl}$ (figure B1). For optical path A_1, we have

$$\begin{aligned} L_s^{(1)} &= L_s \\ R_s^{(1)} &= d_s + \frac{\lambda_i}{\lambda_s} D_i \equiv R_s \\ z_s^{(1)} &= d_s + D_i \equiv z_s, \end{aligned} \tag{B.17}$$

and for optical path A_2

$$\begin{aligned} L_s^{(2)} &= L_s \\ R_s^{(2)} &= (d_s + 2\delta) + \frac{\lambda_i}{\lambda_s} D_i \equiv R_s + 2\delta \\ z_s^{(2)} &= (d_s + 2\delta) + D_i \equiv z_s + 2\delta, \end{aligned} \tag{B.18}$$

where δ is the optical path difference of the reflected optical photon. The refraction effect could be taken into account by employing the dynamical theory of diffraction, which treats the refraction effect explicitly and results in a shift of Laue point that depends on the refractive index of the crystal [18]. Denote the refractive index as $n = 1 - n' - in''$, where $n' < 0$ for optical photons, the refractive index has a relation with the electric susceptibility $n = \sqrt{1 + 4\pi\chi}$ [19], and χ can be determined by *ab initio* means for each atomic species at a given wavelength. The optical path difference could be then expressed as $\delta = \frac{d \sin^2\theta - n'}{\sqrt{\sin^2\theta + 4\pi\chi}}$. Note that the refraction effect could be neglected for the coherent diffractive imaging of single molecules, as shown in appendix C. Thus the effective two-photon joint detection amplitude consists of contributions from the two optical paths, $V(\vec{\rho}_A, \vec{\rho}_B) = V^{(1)}(\vec{\rho}_A, \vec{\rho}_B) + V^{(2)}(\vec{\rho}_A, \vec{\rho}_B)$, and $t(\vec{\rho}_a) = t^{(1)}(\vec{\rho}_a) + t^{(2)}(\vec{\rho}_a) = \psi_0[\delta(\vec{\rho}_a) + \delta(\vec{\rho}_a - \vec{d})]$, where $\vec{d} = (d, 0)$. We write $V^{(1)}(\vec{\rho}_A, \vec{\rho}_B)$ and $V^{(2)}(\vec{\rho}_A, \vec{\rho}_B)$ explicitly as

$$\begin{aligned} V^{(1)}(\vec{\rho}_A, \vec{\rho}_B) &= \frac{\psi_0 e^{iK_s z_s}}{2\pi i \lambda_s R_s} G\left(|\vec{\rho}_A|, \frac{K_s}{L_s}\right) G\left(|\vec{\rho}_B|, \frac{K_s}{R_s}\right) \\ V^{(2)}(\vec{\rho}_A, \vec{\rho}_B) &= \frac{\psi_0 e^{iK_s(z_s+2\delta)}}{2\pi i \lambda_s (R_s + 2\delta)} \\ &\quad \times G\left(|\vec{\rho}_A|, \frac{K_s}{L_s}\right) G\left(|\vec{\rho}_B|, \frac{K_s}{R_s + 2\delta}\right) \\ &\quad \times \left\{ G\left(|\vec{d}|, K_s\left(\frac{1}{L_s} + \frac{1}{R_s + 2\delta}\right)\right) \right. \\ &\quad \left. \times e^{-iK_s\left(\frac{\vec{\rho}_B}{R_s+2\delta} + \frac{\vec{\rho}_A}{L_s}\right)\vec{d}} \right\}. \end{aligned} \tag{B.19}$$

Define $W^{(p)}(\vec{\rho}_B) = \int d^2\vec{\rho}_A V^{(p)}(\vec{\rho}_A, \vec{\rho}_B)$, we have

$$\begin{aligned} W^{(1)}(\vec{\rho}_B) &= \frac{\psi_0 L_s}{2\pi R_s} e^{iK_s z_s} G\left(|\vec{\rho}_B|, \frac{K_s}{R_s}\right) \\ W^{(2)}(\vec{\rho}_B) &= \frac{\psi_0 e^{iK_s(z_s+2\delta)}}{2\pi i \lambda_s (R_s + 2\delta)} G\left(|\vec{\rho}_B|, \frac{K_s}{R_s}\right) e^{-i\frac{K_s\delta}{R_s^2}|\vec{\rho}_B|^2} \\ &\quad \times e^{i\frac{K_s}{2}\left(\frac{1}{L_s} + \frac{1}{R_s}\right)|\vec{d}|^2} e^{-i\frac{K_s\delta}{R_s^2}|\vec{d}|^2} \\ &\quad \times e^{-iK_s\frac{\vec{\rho}_B}{R_s}\cdot\vec{d}} e^{i\frac{2K_s\delta}{R_s^2}\vec{\rho}_B\cdot\vec{d}} \int d^2\vec{\rho}_A G\left(|\vec{\rho}_A|, \frac{K_s}{L_s}\right) e^{-iK_s\frac{\vec{d}}{L_s}\cdot\vec{\rho}_A} \\ &= \frac{\psi_0 L_s}{2\pi R_s} e^{iK_s z_s} G\left(|\vec{\rho}_B|, \frac{K_s}{R_s}\right) e^{i\frac{K_s}{2R_s}(|\vec{d}|^2 - 2\vec{\rho}_B\cdot\vec{d})} \\ &\quad \times e^{iK_s\left[2\delta\left(1 - \frac{|\vec{\rho}_B - \vec{d}|^2}{2R_s^2}\right)\right]}. \end{aligned} \tag{B.20}$$

Take far-field approximation $\delta \ll R_s$ that is similar to the treatment of Laue diffraction (see appendix C), we have

$$\begin{aligned} |W(\vec{\rho}_B)|^2 &= \left| \int d^2\vec{\rho}_A V(\vec{\rho}_A, \vec{\rho}_B) \right|^2 \\ &= \left(\frac{\psi_0 L_s}{2\pi R_s}\right)^2 \{2 + e^{i\frac{K_s}{2R_s}(|\vec{d}|^2 - 2\vec{\rho}_B\cdot\vec{d})} \\ &\quad \times e^{iK_s[2\delta(1 - \frac{|\vec{\rho}_B - \vec{d}|^2}{2R_s^2})]} + \text{c.c.}\}. \end{aligned} \tag{B.21}$$

Analogous to the procedure in appendix C, we obtain the modified Bragg equation for two-color two-photon ghost diffraction from equation (B.21) by requiring the δ-dependent phase to vanish, i.e.

$$\begin{aligned} & K_s\left[2\delta\left(1 - \frac{|\vec{\rho}_B - \vec{d}|^2}{2R_s^2}\right)\right] = 2n\pi \\ \Rightarrow & \frac{2d(\sin^2\theta - n')}{\sqrt{\sin^2\theta + 4\pi\chi}}\left[1 - \frac{|\vec{\rho}_B - \vec{d}|^2}{2\left(\frac{d_s}{D_i} + \frac{\lambda_i}{\lambda_s}\right)^2 D_i^2}\right] = n\lambda_s, \end{aligned} \tag{B.22}$$

with an integer n. Define the magnification factor $\tilde{m}$ as

$$\tilde{m} \equiv \tilde{m}(\vec{\rho}_B, \vec{d}, d_s, D_i, \lambda_i, \lambda_s) = 1 - \frac{|\vec{\rho}_B - \vec{d}|^2}{2\left(\frac{d_s}{D_i} + \frac{\lambda_i}{\lambda_s}\right)^2 D_i^2}. \tag{B.23}$$

The modified Bragg equation can be then written as

$$\frac{2\tilde{m}d(\sin^2\theta - n')}{\sqrt{\sin^2\theta + 4\pi\chi}} = n\lambda_s, \tag{B.24}$$

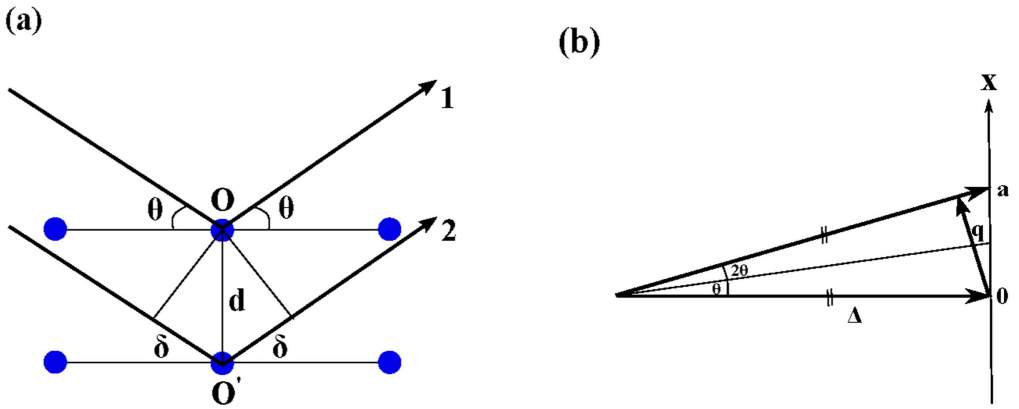

Figure C1. (a) Optical path diagram for Laue diffraction. O and O' are the positions of the atoms in adjacent crystal planes, θ is the reflection angle, and δ denotes the optical path length difference. (b) Momentum relation of Laue diffraction. Δ is the optical path length of the incident and scattered photons along their momentum vectors, and $\vec{q}$ is the momentum transfer.

which reduces to the form $2\tilde{m}d\sin\theta = n\lambda_s$ for $n \simeq 1$, i.e. $n' \ll 1$ and $\chi \ll 1$. Provided that the modified Bragg condition is satisfied, and define $\vec{\rho}_B = (x, 0)$ and $\vec{d} = (d, 0)$ for simplicity, we find

$$\begin{aligned}|W(\vec{\rho}_B)|^2 &= \left|\int \mathrm{d}^2\vec{\rho}_A V(\vec{\rho}_A, \vec{\rho}_B)\right|^2 \\ &= \left(\frac{\psi_0 L_s}{\pi R_s}\right)^2 \cos^2\left[\frac{2\pi}{\lambda_s R_s} d\left(x - \frac{d}{2}\right)\right] \end{aligned} \tag{B.25}$$

which forms a broad and flat background. Using equations (B.1), (B.7), (B.15) and (B.25), we reach the final equation for the counting rate of joint photon detection

$$\begin{aligned}R_c(\vec{\rho}_B) &= \frac{1}{T}\int \mathrm{d}t_A \mathrm{d}t_B S(t_B, t_A)\frac{\sigma_B\gamma^2}{\lambda_s^2 L_s^2} \\ &\quad\times \left|\int \mathrm{d}\nu_S \mathrm{e}^{\mathrm{i}\nu_s\tau_{BA}}\mathrm{sinc}\left(\nu_s D_{si}\frac{L}{2}\right)\right|^2 \\ &\quad\times \left|\int \mathrm{d}^2\vec{\rho}_A V(\vec{\rho}_A, \vec{\rho}_B)\right|^2 \\ &= \frac{1}{T}\int \mathrm{d}t_A \mathrm{d}t_B S(t_B, t_A)\sigma_B\left(\frac{\gamma\psi_0}{\pi\lambda_s R_s}\right)^2 \\ &\quad\times \left|\int \mathrm{d}\nu_S \mathrm{e}^{\mathrm{i}\nu_s\tau_{BA}}\mathrm{sinc}\left(\nu_s D_{si}\frac{L}{2}\right)\right|^2 \\ &\quad\times \cos^2\left[\frac{2\pi}{\lambda_s R_s} d\left(x - \frac{d}{2}\right)\right]. \end{aligned} \tag{B.26}$$

Equation (10) can be simplified using the relation

$$\begin{aligned}&\int_{-\infty}^{\infty} \mathrm{d}\nu_s \mathrm{e}^{\mathrm{i}\nu_s\tau_{BA}}\mathrm{sinc}\left(\nu_s D_{si}\frac{L}{2}\right) \\ &= \frac{2\pi}{D_{si}L}\mathrm{rect}\left(\frac{2\tau_{AB}}{D_{si}L}\right) \\ &= \begin{cases} \frac{2\pi}{D_{si}L} & \text{for } -\frac{D_{si}L}{2} \leqslant \tau_{AB} \leqslant \frac{D_{si}L}{2} \\ 0 & \text{for } |\tau_{AB}| > \frac{D_{si}L}{2} \end{cases}, \end{aligned}$$

and the counting rate of joint detection can be written as

$$\begin{aligned}R_c(\vec{\rho}_B) &= \frac{1}{T}\int \mathrm{d}t_A \mathrm{d}t_B S(t_B, t_A)\sigma_B\left(\frac{2\gamma\psi_0}{D_{si}L\lambda_s R_s}\right)^2 \mathrm{rect}\left(\frac{2\tau_{AB}}{D_{si}L}\right) \\ &\quad\times \cos^2\left[\frac{2\pi}{\lambda_s R_s} d\left(x - \frac{d}{2}\right)\right]. \end{aligned} \tag{B.27}$$

Appendix C. Kinematic description of Laue diffraction

In appendix B, the modified Bragg condition for the two-color two-photon ghost diffraction is obtained from a kinematic scenario. Here we show the conventional Bragg equation can be obtained from similar procedure for the Laue diffraction with monochromatic x-ray beam.

According to the Huygens principle, a light wave that passes the plane $z = 0$, and arrives at the plane $z = \Delta$ can be described as

$$\begin{aligned}E(x, y, \Delta) &= \int \mathrm{d}k_x \mathrm{d}k_y \mathrm{e}^{\mathrm{i}(k_x x + k_y y)}\mathrm{e}^{\mathrm{i}k_z\Delta}\mathcal{F}[E(x, y, 0)] \\ &= \int \mathrm{d}k_x \mathrm{d}k_y \mathrm{e}^{\mathrm{i}(k_x x + k_y y)}\mathrm{e}^{\mathrm{i}\Delta\sqrt{k^2 - k_x^2 - k_y^2}}\breve{E}(k_x, k_y, 0) \\ &\simeq \int \mathrm{d}k_x \mathrm{d}k_y \mathrm{e}^{\mathrm{i}(k_x x + k_y y)}\mathrm{e}^{\mathrm{i}\Delta\left(k - \frac{k_x^2 + k_y^2}{2k}\right)}\breve{E}(k_x, k_y, 0) \\ &= \mathcal{F}^{-1}\{\mathrm{e}^{\mathrm{i}\Delta\left(k - \frac{k_x^2 + k_y^2}{2k}\right)}\breve{E}(k_x, k_y, 0)\} \\ &= E(x, y, 0) \otimes P(x, y, \Delta), \end{aligned} \tag{C.1}$$

where $P(x, y, \Delta)$ is

$$\begin{aligned}P(x, y, \Delta) &= \mathcal{F}^{-1}\{\mathrm{e}^{\mathrm{i}\Delta k}\mathrm{e}^{\mathrm{i}\Delta\left(\frac{k_x^2 + k_y^2}{2k}\right)}\} \\ &= -\frac{\mathrm{i}k\mathrm{e}^{\mathrm{i}k\Delta}}{2\pi\Delta}\mathrm{e}^{\mathrm{i}\frac{k(x^2 + y^2)}{2\Delta}}. \end{aligned} \tag{C.2}$$

The physical scenario of equation (C.1) reflects a typical statement of Huygens principle, that (a) the Fourier transformation on the $z = 0$ plane makes a map to the momentum space

$E(x, y, 0) \rightarrow \breve{E}(k_x, k_y, 0)$, (b) each Fourier mode $\breve{E}(k_x, k_y, 0)$ corresponds to a sub-source that travels as a plane wave $e^{i(k_x x + k_y y)} e^{ik_z \Delta}$ to the $z = \Delta$ plane, and (c) an inverse Fourier transformation on the $z = \Delta$ plane gives the image $E(x, y, \Delta)$. For Laue diffraction, we follow a standard treatment by considering two optical paths 1 and 2 for photons that scatter off atoms in two lattice planes (figure C1(a)). Assume the photon scatters off the two atoms O and O' with amplitude $t^{(1)} = \psi_0 \delta(x - d, y, 0)$ and $t^{(2)} = \psi_0 \delta(x, y, 0)$, and denote $\delta = d \sin\theta$, we have

$$\begin{aligned} E_1(x, y, \Delta) &= \psi_0 \otimes P(x - 0, y - d, \Delta) \\ &= -\frac{ik\psi_0 e^{ik\Delta}}{2\pi\Delta} e^{i\frac{k}{2\Delta}[x^2 + (y-d)^2]} \\ E_2(x, y, \Delta) &= \mathcal{F}^{-1}\left\{ e^{ik_z\delta}\left[\int dx' dy' e^{-i(k_x x' + k_y y')} \psi_0 \delta(x', y', 0)\right] \right. \\ &\quad \left. \times e^{ik(\Delta+\delta)} e^{-i(\Delta+\delta)\left(\frac{k_x^2 + k_y^2}{2k}\right)} \right\} \\ &= -\frac{ik\psi_0 e^{ik(\Delta+2\delta)}}{2\pi(\Delta + 2\delta)} e^{i\frac{k}{2(\Delta+2\delta)}(x^2+y^2)}. \end{aligned} \tag{C.3}$$

Thus the intensity of diffraction pattern $I(x)$ at the detector plane is given by

$$\begin{aligned} I(x) &= |E(x, y, \Delta)|^2 = |E_1(x, y, \Delta) + E_2(x, y, \Delta)|^2 \\ &= \left(\frac{k\psi_0}{2\pi}\right)^2 \left\{ \frac{1}{\Delta^2} + \frac{1}{(\Delta + 2\delta)^2} + \frac{1}{\Delta(\Delta + \delta)} \right. \\ &\quad \left. \times \left[e^{i\frac{\pi}{\lambda}\left[\frac{(x-d)^2}{\Delta} - \frac{x^2}{\Delta+2\delta}\right]} e^{-i\frac{2\pi}{\lambda}2\delta} + \text{c.c.} \right] \right\} \\ &= \left(\frac{k\psi_0}{2\pi}\right)^2 I_1. \end{aligned} \tag{C.4}$$

For far-field diffraction $\Delta \gg 2\delta$, we have

$$\begin{aligned} I_1 &\simeq \frac{1}{\Delta^2}\left\{ 2 + 2\cos\left[\frac{\pi}{\lambda\Delta}[(x - d)^2 - x^2] - \frac{2\pi}{\lambda} 2\delta \right] \right\} \\ &= \frac{2}{\Delta^2}\left\{ 1 + \cos\left[\frac{\pi}{\lambda\Delta} d(d - 2x) - \frac{2\pi}{\lambda} 2\delta \right] \right\} \\ &= \left(\frac{2}{\Delta}\right)^2 \cos^2\left[\frac{\pi}{\lambda\Delta} d\left(x - \frac{d}{2}\right) - \frac{\pi}{\lambda} 2\delta \right], \end{aligned} \tag{C.5}$$

using the relation $1 + \cos\alpha = 2\cos^2\frac{\alpha}{2}$.

The Bragg condition is obtained by requiring the δ-dependent phase in equation (C.5) to vanish,

$$2\delta = 2d \sin\theta = n\lambda. \tag{C.6}$$

We obtain the diffraction pattern on the detector at the distance Δ from the sample,

$$I(x) = \left(\frac{k\psi_0}{\pi\Delta}\right)^2 \cos^2\left[\frac{\pi}{\lambda\Delta} d\left(x - \frac{d}{2}\right) \right], \tag{C.7}$$

with a period $a = \frac{2\lambda\Delta}{d}$.

Meanwhile, we show that the kinematic description is consistent with the description of Laue diffraction in momentum space. The form factor $f(\vec{Q})$ is the Fourier transformation of the charge distribution. For simplicity, we model the atoms as point charges, thus

$$f(\vec{Q}) = \int d\vec{r} e^{i\vec{Q}\cdot\vec{r}} [\delta(\vec{r}) + \delta(\vec{r} - \vec{d})] = 1 + e^{iQd}, \tag{C.8}$$

and the intensity of diffraction pattern is

$$I \sim |f(\vec{Q})|^2 = 2(1 + \cos Qd) = 4\cos^2\frac{Qd}{2}. \tag{C.9}$$

From figure C1(b), we can find that $\sin\theta \simeq \frac{x}{2\Delta}$ and

$$Q \equiv |\vec{Q}| = 2|\vec{k}| \sin\theta \simeq 2\frac{2\pi}{\lambda}\frac{x}{2\Delta} = \frac{2\pi x}{\lambda\Delta}. \tag{C.10}$$

Taken equations (C.9) and (C.10), we obtain the intensity of diffraction pattern

$$I(x) \sim |f(\vec{Q})|^2 = 4\cos^2\left(\frac{\pi d}{\lambda\Delta} x\right), \tag{C.11}$$

with a period $a = \frac{2\lambda\Delta}{d}$, which is consistent with equation (C.7) from the kinematic description of Laue diffraction.

Intriguingly, the kinematic description of diffraction can be directly used for a Gedanken experiment, which could reveal the essence of the proposed ghost diffraction effect and the origin of the subdiffraction limit resolution. The ghost diffraction relies essentially on the optical Thomson scattering from the atoms in molecules and crystals. Consider the Thomson scattering from a hydrogen-like molecule with two electrons and bond length R of several Ångstrom, it is equivalent to the coherent diffractive imaging from this molecule [15]. Assume the incident light has an optical wavelength λ, and $\lambda/2 \gg R$, the wave vectors of the incident and the scattered wave are $\vec{k}$ and $\vec{k}'$, for simplicity, the polarization is perpendicular to the $(\vec{k}, \vec{k}')$ plane, and we take electrons as classical point charges in the simplest case. As shown in appendix A, the expression of Thomson scattering cross section remains intact at optical wavelengths. The wave vector transfer of elastic Thomson scattering is $|\vec{Q}| = |\vec{k}' - \vec{k}| = \frac{4\pi}{\lambda}\sin\theta$, and the scattering amplitude from the two-electron molecule can be written as

$$A(\vec{Q}, \vec{R}) = -r_e(1 + e^{i\vec{Q}\cdot\vec{R}}), \tag{C.12}$$

and the intensity is thus $I(\vec{Q}, \vec{R}) = |A(\vec{Q}, \vec{R})|^2 = 2r_e^2[1 + \cos(\vec{Q}\cdot\vec{R})]$, where r_e is the classical electron radius. Because the scattering amplitude $A(\vec{Q}, \vec{R})$ is a function of bond length R, it carries in fact the structure information of the molecule below the diffraction limit. The actual problem is that for $Q = \frac{4\pi}{\lambda}\sin\theta$, no diffraction peak can be formed from the intensity distribution $I(\vec{Q}, \vec{R})$ as a function of the scattering angle 2θ, thus it is impossible to acquire the bond length R from observables of measurement of first-order optical coherence. In this sense, the essence of the ghost diffraction method is to extract the quantity R with the entangled x-ray photon and the corresponding measurement of second-order optical coherence, as described in equation (3) of the main text. Note that a more realistic treatment to consider the electrons as quantum particles results in an atomic form factor in the expression of

intensity distribution $I(\vec{Q},\vec{R}) = 2|f(\vec{Q})|^2[1+\cos(\vec{Q}\cdot\vec{R})]$. For hydrogen-like wave function $\psi(\vec{r}) = \frac{1}{\sqrt{\pi a^3}}e^{-r/a}$, we have $f(\vec{Q}) = \frac{1}{[1+(Qa/2)^2]^2}$, where $a = a_0/Z'$, a_0 is the Bohr radius and Z' is the screened nuclear charge. The conclusion from the classical point charge electron model remains intact—Thomson scattering at optical wavelength can carry atomic scale structure information and give nonzero intensity at the detector plane.

Appendix D. Broadening of Bragg peaks

Analogous to the Scherrer equation, we calculate the width of the Bragg peaks of the two-color two-photon ghost diffraction, which determines the resolution of the proposed scheme. It is especially important for the application of XFELs to the diffraction of nanocrystals with a finite size. Supposing a nanocrystal of length L_c that contains N lattice planes with inter-plane distance d, such that $Nd = L_c$, the accumulated δ-dependent phase for the diffraction from N atoms can be calculated using equation (B.21) as

$$\begin{aligned}\Gamma(\theta) &= \sum_{p=0}^{N-1} e^{ipK_s\left[2\delta\left(1-\frac{|\vec{\rho}_B-\vec{d}|^2}{2R_s^2}\right)\right]} \\ &= Ne^{i\frac{N-1}{2}K_s(2\tilde{m}\delta)}\mathrm{sinc}\left[\frac{N}{2}K_s(2\tilde{m}\delta)\right],\end{aligned} \tag{D.1}$$

where $\delta = \frac{d\sin^2\theta - n'}{\sqrt{\sin^2\theta+4\pi\chi}}$. Thus the line shape $\mathcal{L}(\theta)$ of a Bragg peak at a reflection angle θ is

$$\mathcal{L}(\theta) = \Gamma^2(\theta) = N^2\mathrm{sinc}^2\left[\frac{N}{2}K_s(2\tilde{m}\delta)\right]. \tag{D.2}$$

The width of the Bragg peak can be then found through zeros of the line shape function as

$$\frac{N}{2}K_s\left[\frac{2\tilde{m}d\sin\theta\cos\theta}{(\sin^2\theta+4\pi\chi)^{\frac{3}{2}}}\left(\sin^2\theta+4\pi\chi+\frac{n'}{2}\right)\right]\Delta\theta = 2\pi. \tag{D.3}$$

Defining the width of the Bragg peak as $B = 2\Delta\theta$, we find

$$B = \frac{2\lambda_s(\sin^2\theta+4\pi\chi)^{\frac{3}{2}}}{L_c\tilde{m}\sin\theta\cos\theta(\sin^2\theta+4\pi\chi+\frac{n'}{2})}. \tag{D.4}$$

The factor $\frac{\lambda_s}{\tilde{m}}$ in the width of Bragg peaks guarantees that the two-color two-photon ghost diffraction will have a similar resolution as the Laue diffraction, i.e. on the atomic scale.

Appendix E. X-ray parametric down-conversion (XPDC) through nonlinear crystal and single electron

In this section, we present details of the two proposed schemes for XPDC using conventional nonlinear crystals or single electron as the nonlinear medium. We also present an estimation of the efficiency from experimental consideration for the XPDC of an x-ray photon of frequency ω_{X3} to a pair of x-ray and optical photons of frequencies ω_{X2} and ω_{o1}. Both schemes rely dominantly on the figure-eight motion of electrons turned by Lorentz force. For the nonlinear crystal based XPDC, the phase-matching condition relies critically on the well-defined lattice vectors of reciprocal space, thus the structural damage to the crystal inevitably causes deterioration of the XPDC process. Moreover the conventionally used crystals, like diamond, can strongly absorb the photons and substantially suppress the XPDC efficiency [8].

In contrast, the XPDC using free electrons and Kapitza–Dirac-like scattering could have the advantage of being free of damage to the nonlinear crystal by the intense x-ray light and strong absorption of the photons inside of the crystal medium.

E.1. XPDC using nonlinear crystal

To obtain an order-of-magnitude estimation of the XPDC cross section by nonlinear crystalline medium, we use a semiclassical formalism to calculate nonlinear response functions for x-rays [24]. For electrons in the atom with density ρ and velocity $\vec{v}$, we apply the equation of motion and continuity condition

$$\begin{aligned}\frac{\partial\vec{v}}{\partial t} + (\vec{v}\cdot\vec{\nabla})\vec{v} &= -\frac{e}{m}\left(\vec{E}+\frac{1}{c}\vec{v}\times\vec{B}\right) \\ \frac{\partial\rho}{\partial t} + \vec{\nabla}\cdot(\rho\vec{v}) &= 0.\end{aligned} \tag{E.1}$$

Under perturbative expansion $\rho = \rho^{(0)}+\rho^{(1)}+\rho^{(2)}+\cdots$, $\vec{v} = \vec{v}^{(1)}+\vec{v}^{(2)}+\cdots$, and $\vec{J} = \vec{J}^{(1)}+\vec{J}^{(2)}+\cdots$, we obtain the second-order nonlinear current for a general XPDC process $\omega_3 \to \omega_1 + \omega_2$

$$\begin{aligned}\vec{J}^{(2)}(\omega_3) &= \rho^{(0)}\vec{v}^{(2)} + \rho^{(1)}\vec{v}^{(1)} \\ &= \rho^{(0)}\frac{e^2}{m^2}\left[\frac{\vec{E}_1\times(\vec{k}_2\times\vec{E}_2)}{\omega_1\omega_2\omega_3} + i\frac{(\vec{E}_1\cdot\vec{\nabla})\vec{E}_2}{\omega_1^2\omega_3}\right] \\ &\quad + \frac{ie^2}{m^2}\frac{(\vec{\nabla}\rho\cdot\vec{E}_2)\vec{E}_1}{\omega_1^2\omega_2} + \text{terms with interchanged index}\end{aligned} \tag{E.2}$$

where the second term vanishes in the case $\vec{E}_1 \perp \vec{k}_2$, since $(\vec{E}_1\cdot\vec{\nabla})\vec{E}_2 = (\vec{E}_1\cdot\vec{k}_2)\vec{E}_2 = 0$.

We now consider the XPDC of a hard x-ray photon to a pair of x-ray and optical photons $\omega_{X3} \to \omega_{o1}+\omega_{X2}$. Physically this process is equivalent to the Thomson scattering of x-rays by an atom illuminated with an optical field, which induces Doppler-shifted sideband [23]. Of the several terms that occur in the second-order current (equation (E.2)) for the nonlinear response of an atom to applied electromagnetic fields of frequencies ω_{o1}, ω_{X2}, ω_{X3}, only one is of importance to the present instance [23, 31],

$$\vec{J}^{(2)}(\omega_{X3}) \simeq \frac{ie^2}{m^2}\frac{(\vec{\nabla}\rho\cdot\vec{E}_{X2})\vec{E}_{o1}}{\omega_{o1}^2\omega_{X2}}, \tag{E.3}$$

where $\omega_{X3} = \omega_{o1} + \omega_{X2}$, and ρ is the electron density of the crystal. Equation (E.3) describes the Doppler-shifted reflection of $\vec{E}_2$ from electron that is driven by the optical field $\vec{E}_1$ and moving with velocity $\vec{v}_1$. For simplicity, we denote thereafter $\omega_{o1} = \omega_1$, $\omega_{X2} = \omega_2$, $\omega_{X3} = \omega_3$, the same notation applies for the momentum k and electromagnetic fields E and B. We expand the electron density in terms of reciprocal lattice vector $\vec{G}_m$ that $\rho(\vec{r}) = \sum_m \rho_m e^{i\vec{G}_m\cdot\vec{r}}$. The dominant nonlinear current is

$$\vec{J}^{(2)}(\omega_3) \simeq -\frac{e^2}{m^2}\sum_m \frac{(\rho_m\cdot\vec{e}_2)\vec{e}_1}{\omega_1^2\omega_2} e^{i[(\vec{k}_1+\vec{k}_2+\vec{G}_m)\cdot\vec{r}-(\omega_1+\omega_2)t]}, \tag{E.4}$$

where $\vec{e}_i$ is the polarization vector of the electric field $\vec{E}_i$. In the general case, the relation between the nonlinear response functions $R^{(n)}$ and the corresponding nonlinear susceptibilities $\chi^{(n)}$ is [24]

$$\chi^{(n)}(\omega;\,\omega_1,\,\omega_2,\cdots,\omega_n) = i^{1-n}\frac{c^n}{\omega_1\omega_2\omega_n}R^{(n)}(\omega;\,\omega_1,\,\omega_2,\cdots,\omega_n). \tag{E.5}$$

For the quadratic process, the nonlinear current is

$$eJ_i^{(2)}(\omega_3) \propto R_{ijk}^{(2)}(\omega_3;\,\omega_1,\,\omega_2)A_j(\omega_1)A_k(\omega_2). \tag{E.6}$$

Since $A(\omega) \sim \frac{cE}{\omega}$, by inspection the nonlinear response function is

$$R^{(2)} \propto \frac{e^3\rho}{m^2c^2\omega_1}. \tag{E.7}$$

The nonlinear susceptibility is thus

$$\chi^2(\omega_3;\,\omega_1,\,\omega_2) \simeq \frac{e^3\rho}{m^2\omega_1^2\omega_2\omega_3} \overset{\text{a.u.}}{=} \frac{\alpha^2 r_e\rho}{k_1^2k_2k_3} \tag{E.8}$$

in atomic units, where α is the fine structure constant and r_e is the classical electron radius. The estimation of $\chi^{(2)}$ in equation (E.8) is consistent with the earlier work (see comment 28 in [32]). Using Fermi's golden rule, we obtain the differential cross section for XPDC as [24]

$$\frac{d\sigma^{(2)}}{d\Omega} = \frac{\omega_3\omega_2^3\omega_1^3}{288\pi^3c^7}|\chi^{(2)}|^2. \tag{E.9}$$

Equations (E.8) and (E.10) give the scaling of cross section as $\propto 1/\omega_1$, which especially favors XPDC to entangled photon pair with a low energy optical photon. For the instance given in the main text of XPDC $\omega_3(=3.1\text{ keV}) \to \omega_2(=3096.9\text{ eV}) + \omega_1(=3.1\text{ eV})$ with diamond crystal, we obtain $\chi^{(2)} \sim 9.1\times10^{-12}\text{cm}^2\,\text{StC}^{-1}$, where StC is the Gaussian unit of StatCoulomb. The XPDC cross section is

$$\frac{d\sigma^{(2)}}{d\Omega} \sim 1.9\times10^3\,\text{fm}^2 = 19\,\text{b}, \tag{E.10}$$

which could be comparable to the cross section of Thomson scattering. Nevertheless, the low XPDC efficiency in actual experiments could be attributed to the radiation damage caused deterioration of phase-matching condition and strong absorption of photons inside the crystal.

We also show here that the (quasi-)degenerate XPDC $\omega_X \to \omega_X/2 + \omega_X/2$ [8] has cross section that is almost four orders of magnitude lower than the XPDC to x-ray and optical photons. In this case $\omega_3 = \omega$ and $\omega_1 = \omega_2 = \omega/2$ are both in the x-ray regime, the dominant nonlinear current is

$$\vec{J}^{(2)}(\omega_3) \simeq \rho^{(0)}\frac{e^2}{m^2}\frac{\vec{E}_1\times(\vec{k}_2\times\vec{E}_2)}{\omega_1\omega_2\omega_3} \simeq \frac{e^2\rho^{(0)}\vec{k}_2E_1E_2}{m^2\omega_1\omega_2\omega_3}. \tag{E.11}$$

Similarly we obtain the nonlinear response function for (quasi)-degenerate XPDC and the nonlinear susceptibility,

$$R^{(2)} \simeq \frac{\rho e^3}{2m^2c^3}$$
$$\chi^{(2)} \simeq \frac{2e^3\rho}{m^2c\omega^3} \overset{\text{a.u.}}{=} \frac{\alpha^2 r_e\rho}{k^3}. \tag{E.12}$$

Taken the experimental parameters in the earlier work [8], $\omega_3(=18\text{keV}) \to \omega_1(=9\text{ keV}) + \omega_2(=9\text{ keV})$ with diamond crystal, we obtain $\chi^{(2)} \sim 7.7\times10^{-20}\,\text{cm}^2\,\text{StC}^{-1}$, and the XPDC cross section is

$$\frac{d\sigma^{(2)}}{d\Omega} \sim 4.7\times10^{-3}\,\text{b}, \tag{E.13}$$

which is lower than the cross section in equation (E.10) by four orders of magnitude.

E.2. XPDC using single electron

The XPDC process is essentially different from the SPDC process of optical photons in the dominant nonlinear motion. The nonlinear currents that stem from the quivering motion of bound electrons subject to anharmonic potential and the figure-eight motion driven by Lorentz force has the relation

$$\frac{J^{(2)}_{\text{anharmonic}}}{J^{(2)}_{\text{figure-8}}} = \frac{\lambda}{2\pi d}\frac{\omega_0^2}{\omega^2},$$

where d is the lattice spacing and ω_0 is frequency of atomic resonance, λ and ω are the wavelength and frequency of the driving light field, respectively. It is obvious that for x-rays with $\omega \gg \omega_0$, the nonlinear currents have the relation $J^{(2)}_{\text{anharmonic}} \ll J^{(2)}_{\text{figure-8}}$. The electrons in crystal behaves in fact similarly as quasi-free electrons in the x-ray field, and follow the figure-eight trajectory [33, 34]

$$x = -\frac{a^2}{8k(1+a^2/2)}\sin 2\phi$$
$$z = \frac{a}{k\sqrt{1+a^2/2}}\cos\phi,$$

as it is driven by a monochromatic x-ray field, where x and z are the propagation and polarization direction of the x-ray

light field, $a = \frac{A}{c}$ is the amplitude of dimensionless vector potential of the light, and $\phi = \omega t - kx$ is the phase. Note that the phase is actually proportional to the proper time of the co-moving system, $\phi \propto \tau$, but not the time t in the lab system, thus harmonics of all orders can appear from the figure-eight motion. Based on the observation above, it is clear that the free electrons can directly play the role of the nonlinear medium without the anharmonic bound potential provided by atoms in a crystal. Thus we could use the beam of single electrons for XPDC, as depicted in figure 5. A linearly polarized x-ray field (ω_{X3}, k_{X3}) propagates from the right along the x axis, while two seeding fields (ω_{o1}, k_{o1}) and (ω_{X2}, k_{X2}) propagate from the left along the x axis, and $\omega_{o1} + \omega_{X2} = \omega_{X3}$, $k_{o1} + k_{X2} = k_{X3}$. The electric fields E_{o1}, E_{X2}, E_{X3} are polarized along the z axis. The figure-eight motion of the electron in the fields of E_{o1} and E_{X2} creates polarization along the x axis $P_x^{(2)}(\omega_{X3}) = \chi_{xzz}^{(2)}(\omega_{X3};\, \omega_{o1},\, \omega_{X2}) E_{o1,z} E_{X2,z}$. Meanwhile the x-ray field of ω_{X3} induces polarization $P_x^{(1)}(\omega_{X3}) = \chi_{xz}^{(1)}(\omega_{X3};\, \omega_{X3}) E_{X3}$. The two wave mixing of $P^{(2)}(\omega_{X3})$ and $P^{(2)}(\omega_{X3})$ induces the effective grating for diffractive scattering of the electron with Bragg angle $\sin\theta_B = \frac{k_{X3}}{p_i}$ (figure 5), where $_{pi}$ is the initial momentum of the electron [35]. From the perspective of nonlinear optics, this three-color Kapitza–Dirac-like scattering is an XPDC process, in which the electron absorbs an x-ray photon of ω_{X3}, converts it to a pair of photons with ω_{o1}, ω_{X2} and changes the momentum by 2 k_{X3} for momentum conservation. Since we use photons of frequencies ω_{o1} and ω_{X2} as seeding photons, we could eventually identify the entangled photon pair from XPDC by coincidence with the deflected electron.

In the following, we present a quantum-classical approach [27, 33] to obtain the probability of the three-color Kapitza–Dirac-like XPDC process $\omega_{X3} \rightarrow \omega_{o1} + \omega_{X2}$. For the electron that scatters from the effective grating and transitions from the initial state $|\vec{p}_i\rangle$ to the final state $|\vec{p}_f\rangle = |\vec{p}_i + 2\vec{k}_{X3}\rangle$, we calculate the periodic stationary potential of the grating and obtain the transition probability. Similar to E.1, we denote thereafter $\omega_{o1} = \omega_1$, $\omega_{X2} = \omega_2$, $\omega_{X3} = \omega_3$, the same indices apply for the momentum k and electromagnetic fields E and B. For the mixed waves, the electric field $\vec{E} = (0,\, 0,\, E(x,\, t))$ is

$$E(x,\, t) = E_1 \cos(\omega_1 t - k_1 x) + E_2 \cos(\omega_2 t - k_2 x) + E_3 \cos(\omega_3 t + k_3 x). \tag{E.14}$$

Faraday's law $\vec{\nabla} \times \vec{E} = -\frac{1}{c}\frac{\partial \vec{B}}{\partial t}$ gives the magnetic field $\vec{B} = (0,\, B(x,\, t),\, 0)$ with

$$B(x,\, t) = E_1 \cos(\omega_1 - k_1 x) + E_2 \cos(\omega_2 t - k_2 x) - E_3 \cos(\omega_3 + k_3 x). \tag{E.15}$$

The classical equations of motion of the electron in the electromagnetic field are

$$\ddot{x} = \frac{\dot{z}}{c} B(x,\, t), \tag{E.16}$$

$$\ddot{z} = -E(x,\, t) - \frac{\dot{x}}{c} B(x,\, t). \tag{E.17}$$

We separate the motion along x and z axis into fast and slow components, $x = x_f + x_s$, $z = z_f + z_s$, where the slow component corresponds to the electron motion across the laser focus, and the fast component corresponds to the oscillation of the electron in the light field. Applying Taylor expansion around x_s and z_s, the equations of motion become

$$\ddot{x} \simeq \frac{\dot{z}}{c}\left[B(x_s,\, t) + x_f \frac{\partial B(x_s,\, t)}{\partial x_s}\right], \tag{E.18}$$

$$\ddot{z} \simeq -E(x_s,\, t) - x_f \frac{\partial E(x_s,\, t)}{\partial x_s} - \frac{\dot{x}}{c}\left[B(x_s,\, t) + x_f \frac{\partial B(x_s,\, t)}{\partial x_s}\right]. \tag{E.19}$$

Note that equation (E.17) is full derivative with respect to time, integrate it once we get

$$\dot{z} = v_z - 2\left[\frac{E_1}{\omega_1}\sin(\omega_1 t - k_1 x) - \frac{E_2}{\omega_2}\sin(\omega_2 t - k_2 x) - \frac{E_3}{\omega_3}\sin(\omega_3 t + k_3 x)\right]. \tag{E.20}$$

Insert $\dot{z}$ of equation (E.20) into right-hand side (rhs) of equation (E.18), and integrate twice over time, we obtain the trajectory of $x(t)$. We inspect equation (E.18), keeping the rhs of equation (E.18) to the leading order of $\mathcal{O}(\dot{z}_s/c)$, the only possible terms in the bracket $[\cdots]$ that are independent of t must rise from the product of second-order terms in x and the first-order terms in $\frac{B(x_s,\, t)}{\partial x_s}$, because the $\omega_i t$ variables can then cancel with each other due to energy conservation condition $\omega_1 + \omega_2 = \omega_3$. We collect fast oscillating terms in $\ddot{x}$ of equation (E.16) that can lead to cancellation of the time variable, that

$$\begin{aligned}\ddot{x}_f = &-\frac{E_1 E_2}{\omega_1 c}\sin[(\omega_1 + \omega_2)t - (k_1 + k_2)x_s] \\ &-\frac{E_1 E_3}{\omega_1 c}\sin[(\omega_3 - \omega_1)t + (k_3 + k_1)x_s] \\ &-\frac{E_2 E_1}{\omega_2 c}\sin[(\omega_1 + \omega_2)t - (k_1 + k_2)x_s] \\ &-\frac{E_2 E_3}{\omega_2 c}\sin[(\omega_3 - \omega_2)t + (k_3 + k_2)x_s] \\ &-\frac{E_3 E_1}{\omega_3 c}\sin[(\omega_3 - \omega_1)t + (k_3 + k_1)x_s] \\ &-\frac{E_3 E_2}{\omega_3 c}\sin[(\omega_3 - \omega_2)t + (k_3 + k_2)x_s] \\ &+ \mathcal{R},\end{aligned} \tag{E.21}$$

where $\mathcal{R}$ stands for the residual terms that lead to non-stationary potentials. From equation (E.21) it is straightforward to obtain

$$
\begin{aligned}
x_f = & \frac{E_1E_2}{\omega_1(\omega_1+\omega_2)^2c}\sin[(\omega_1+\omega_2)t-(k_1+k_2)x_s] \\
& + \frac{E_1E_3}{\omega_1(\omega_3-\omega_2)^2c}\sin[(\omega_3-\omega_1)t+(k_3+k_1)x_s] \\
& + \frac{E_2E_1}{\omega_2(\omega_1+\omega_2)^2c}\sin[(\omega_1+\omega_2)t-(k_1+k_2)x_s] \\
& + \frac{E_2E_3}{\omega_2(\omega_3-\omega_2)^2c}\sin[(\omega_3-\omega_2)t+(k_3+k_2)x_s] \\
& + \frac{E_3E_1}{\omega_3(\omega_3-\omega_1)^2c}\sin[(\omega_3-\omega_1)t+(k_3+k_1)x_s] \\
& + \frac{E_3E_2}{\omega_3(\omega_3-\omega_2)^2c}\sin[(\omega_3-\omega_2)t+(k_3+k_2)x_s] \\
& + \mathcal{R}.
\end{aligned}
\tag{E.22}
$$

Insert equation (E.22) into the term $x_f\frac{\partial B(x_s,t)}{\partial x_s}$ of equation (E.18), and collect the stationary terms

$$
\begin{aligned}
& x_f\frac{\partial B(x_s,t)}{\partial x_s} \\
& = x_f\left[\frac{\omega_1E_1}{c}\sin(\omega_1t-k_1x_s)+\frac{\omega_2E_2}{c}\sin(\omega_2t-k_2x_s)\right. \\
& \quad \left.+\frac{\omega_3E_3}{c}\sin(\omega_3t+k_3x_s)\right] \\
& = \frac{E_1E_2E_3}{c^2}\left(\frac{1}{\omega_1\omega_3}+\frac{1}{\omega_1\omega_2}+\frac{1}{\omega_2\omega_3}\right) \\
& \quad \times\cos[(k_1+k_2+k_3)x_s]+\mathcal{R}.
\end{aligned}
\tag{E.23}
$$

Thus we have the equation of motion for the electron to travel across the light field,

$$
\begin{aligned}
\ddot{x}_s = & \frac{z_s}{c^3}E_1E_2E_3\left(\frac{1}{\omega_1\omega_3}+\frac{1}{\omega_1\omega_2}+\frac{1}{\omega_2\omega_3}\right) \\
& \times\cos[(k_1+k_2+k_3)x_s].
\end{aligned}
\tag{E.24}
$$

Solving $\ddot{z}_s$ similarly and integrating once, we obtain

$$
\begin{aligned}
\dot{z}_s = & v_z-\frac{E_1E_2E_3}{8\omega_3c^2}\left(\frac{1}{\omega_1\omega_3}+\frac{1}{\omega_1\omega_2}+\frac{1}{\omega_2\omega_3}\right) \\
& \times\sin[(k_1+k_2+k_3)x_s],
\end{aligned}
\tag{E.25}
$$

where v_z is the initial velocity of the electron along the z axis. With equations (E.25) and (E.24) we obtain

$$
\begin{aligned}
\ddot{x}_s = & \frac{v_zE_1E_2E_3}{c^3}\left(\frac{1}{\omega_1\omega_3}+\frac{1}{\omega_1\omega_2}+\frac{1}{\omega_2\omega_3}\right) \\
& \times\cos[(k_1+k_2+k_3)x_s] \\
& -\frac{E_1^2E_2^2E_3^2}{16\omega_3c^5}\left(\frac{1}{\omega_1\omega_3}+\frac{1}{\omega_1\omega_2}+\frac{1}{\omega_2\omega_3}\right)^2 \\
& \times\sin[2(k_1+k_2+k_3)x_s].
\end{aligned}
\tag{E.26}
$$

From the equation of motion for the scattering of the incident electron (equation (E.26)), we can directly deduce the effective stationary periodic potential of the grating as

$$
\begin{aligned}
U_{\text{eff}} = & \frac{v_zE_1E_2E_3}{2\omega_3c^2}\left(\frac{1}{\omega_1\omega_3}+\frac{1}{\omega_1\omega_2}+\frac{1}{\omega_2\omega_3}\right) \\
& \times\sin[(k_1+k_2+k_3)x_s],
\end{aligned}
\tag{E.27}
$$

since the first term in equation (E.26) dominates. Using first-order perturbation theory, the probability of elastic scattering of an incident free electron from $|\vec{p}_i\rangle$ to the final state $|\vec{p}_f\rangle=|\vec{p}_i+2\vec{k}_3\rangle$ is

$$
P(\omega_1,\omega_2,\omega_3)=\left|\frac{v_zE_1E_2E_3}{2c^2\omega_1\omega_2\omega_3}\right|^2\delta(E_{fi}),
\tag{E.28}
$$

where $E_{fi}=p_f^2/2-p_i^2/2$. The schematic setup in sketched in figure 5. To avoid the metal foil filter of being radiated by the intense x-ray field of ω_{X3}, its collinear relation with the counterpropagating seeding fields with ω_{o1} and ω_{X2} can be loosened with respected to the phase-matching condition.

ORCID iDs

Zheng Li https://orcid.org/0000-0002-5483-9149
Nikita Medvedev https://orcid.org/0000-0003-0491-1090

References

[1] Barty A *et al* 2012 Self-terminating diffraction gates femtosecond x-ray nanocrystallography measurements *Nat. Photon.* **6** 35
[2] Spence J 2008 X-ray imaging: ultrafast diffract-and-destroy movies *Nat. Photon.* **2** 390
[3] Nishino Y, Takahashi Y, Imamoto N, Ishikawa T and Maeshima K 2009 Three-dimensional visualization of a human chromosome using coherent x-ray diffraction *Phys. Rev. Lett.* **102** 018101
[4] Quiney H and Nugent K A 2011 Biomolecular imaging and electronic damage using x-ray free-electron lasers *Nature Phys.* **7** 142
[5] Fratalocchi A and Ruocco G 2011 Single-molecule imaging with x-ray free-electron lasers: dream or reality? *Phys. Rev. Lett.* **106** 105504
[6] Glover T E *et al* 2012 X-ray and optical wave mixing *Nature* **488** 603
[7] Tamasaku K, Sawada K, Nishibori E and Ishikawa T 2011 Visualizing the local optical response to extreme-ultraviolet radiation *Nature Phys.* **7** 705
[8] Shwartz S, Coffee R N, Feldkamp J M, Feng Y, Hastings J B, Yin G Y and Harris S E 2012 X-ray parametric down-conversion in the Langevin regime *Phys. Rev. Lett.* **109** 013602
[9] Pittman T B, Shih Y H, Strekalov D V and Sergienko A V 1995 Optical imaging by means of two-photon quantum entanglement *Phys. Rev.* A **52** R3429
[10] Strekalov A, Sergienko A V, Klyshko D N and Shih Y H 1995 Observation of two-photon ghost interference and diffraction *Phys. Rev. Lett.* **74** 3600
[11] Scarcelli G, Berardi V and Shih Y H 2006 Can two-photon correlation of chaotic light be considered as correlation of intensity fluctuations? *Phys. Rev. Lett.* **96** 063602
[12] Rubin M H and Shih Y H 2008 Resolution of ghost imaging for nondegenerate spontaneous parameteric down-conversion *Phys. Rev.* A **78** 033836

[13] Yu H, Lu R, Han S, Xie H, Du G, Xiao T and Zhu D 2016 Fourier-transform ghost imaging with hard x rays *Phys. Rev. Lett.* **117** 113901
[14] Pelliccia D, Rack A, Scheel M, Cantelli V and Paganin D M 2016 Experimental x-ray ghost imaging *Phys. Rev. Lett.* **117** 113902
[15] Als-Nielsen J and McMorrow D 2011 *Elements of Modern x-ray Physics* (New York: Wiley)
[16] Einstein A, Podolsky B and Rosen N 1935 Can quantum-mechanical description of physical reality be considered complete? *Phys. Rev.* **47** 777
[17] Klyshko D N 1988 A simple method of preparing pure states of an optical field, of implementing the Einstein–Podolsky–Rosen experiment, and of demonstrating the complementarity principle *Usp. Fiz. Nauk* **154** 133
[18] Shvyd'ko Y 2013 Dynamical theory of x-ray diffraction *X-ray Optics: High-Energy-Resolution Applications* (Berlin: Springer)
[19] Santra R 2008 Concepts in x-ray physics *J. Phys. B: At. Mol. Opt. Phys.* **42** 023001
[20] Tamasaku K and Ishikawa T 2007 Interference between compton scattering and x-ray parametric down-conversion *Phys. Rev. Lett.* **98** 244801
[21] Van Hove L 1954 Correlations in space and time and born approximation scattering in systems of interacting particles *Phys. Rev.* **95** 249
[22] Adams B W *et al* 2013 X-ray quantum optics *J. Mod. Opt.* **60** 2
[23] Freund I and Levine B F 1970 Optically modulated x-ray diffraction *Phys. Rev. Lett.* **25** 1241–5
[24] Zambianchi P 2003 Nonlinear response functions for x-ray laser pulses *Nonlinear Optics, Quantum Optics, and Ultrafast Phenomena with X-Rays* (Berlin: Springer) pp 287–302
[25] Batelaan H 2007 Colloquium: Illuminating the Kapitza–Dirac effect with electron matter optics *Rev. Mod. Phys.* **79** 929–41
[26] Freimund D L, Aflatooni K and Batelaan H 2001 Observation of the Kapitza–Dirac effect *Nature* **413** 142–3
[27] Smirnova O, Freimund D L, Batelaan H and Ivanov M 2004 Kapitza–Dirac diffraction without standing waves: diffraction without a grating? *Phys. Rev. Lett.* **92** 223601
[28] Son S-K, Chapman H N and Santra R 2011 Multiwavelength anomalous diffraction at high x-ray intensity *Phys. Rev. Lett.* **107** 218102
[29] Long D A 2002 Quantum mechanical theory of Rayleigh and Raman scattering *The Raman Effect: A Unified Treatment of the Theory of Raman Scattering by Molecules* (New York: Wiley) pp 49–84
[30] Rubin M H 1996 Transverse correlation in optical spontaneous parametric down-conversion *Phys. Rev.* A **54** 5349
[31] Freund I 1972 Nonlinear x-ray diffraction. Determination of valence electron charge distributions *Chem. Phys. Lett.* **12** 583
[32] Barbiellini B, Joly Y and Tamasaku K 2015 Explaining the x-ray nonlinear susceptibility of diamond and silicon near absorption edges *Phys. Rev.* B **92** 155119
[33] Fedorov M V 1991 *Electrons in a Strong Laser Field* (Moscow: Nauka)
[34] Sarachik E S and Schappert G T 1970 Classical theory of the scattering of intense laser radiation by free electrons *Phys. Rev.* D **1** 2738
[35] Boyd R 1992 *Nonlinear Optics* (New York: Academic)